

8. MEASUREMENT SUMMARY AND CONCLUSIONS

Robert .J. Matheson¹

8.1 Introduction

This section contains a summary of the measurements made on various UWB devices using the measurement techniques described in Sections 5 and 6. The data presented in this section have been selected from the total measurement set made on each UWB device; additional measurement data for each device is included in Appendix D.

Measurements from six devices are included.

Device A	Section 8.3.1, Appendix D-A
Device B	Section 8.3.2, Appendix D-B
Device C	Section 8.3.3, Appendix D-C
Device D	Section 8.3.4, Appendix D-D
Device E	Section 8.3.5, Appendix D-E
Electric drill	Section 8.3.6, Appendix D-F

8.2 Examples for Detailed Analysis

This section describes the selected measured data in detail, using examples from Devices A, B, and D. It is expected that the reader will apply the explanations to corresponding data from the remainder of the UWB devices, as appropriate. Data for each device will be presented in the same order to facilitate locating data and comparing results between different devices

8.2.1. Device Description

This is a short description of the UWB technology employed. ITS is making no claims that the UWB device works as intended or as described. In most cases, ITS did not functionally test the UWB device performance in any way (except to ascertain that the UWB transmitter was apparently functioning), and consequently ITS is unaware of whether a specific UWB device achieves any of its intended or claimed functional performance objectives.

¹The author is with the Institute for Telecommunication Sciences, National Telecommunications and Information Administration, U.S. Department of Commerce, Boulder, Colorado 80305

Device A uses a 10-kHz pulse repetition rate (PRR), apparently not gated, dithered, or modulated. ITS had no information on the operational aspects of this device (e.g., whether there was any adaptive modification of transmitter modes depending on device location), and testing proceeded on the assumption that the on-off switch was the only significant test variable.

8.2.2. Full-Bandwidth Pulse Shape

Figure 8.1 is an example of a full-bandwidth pulse shape measurement, as described in Section 5. Major objectives of this measurement include understanding full bandwidth pulse shapes, evaluating the possible utility of various pulse-width models for engineering and regulatory purposes (especially to relate pulse shape to the emission spectrum), and furnishing raw data for fast Fourier transform (FFT) computations of emission spectra.

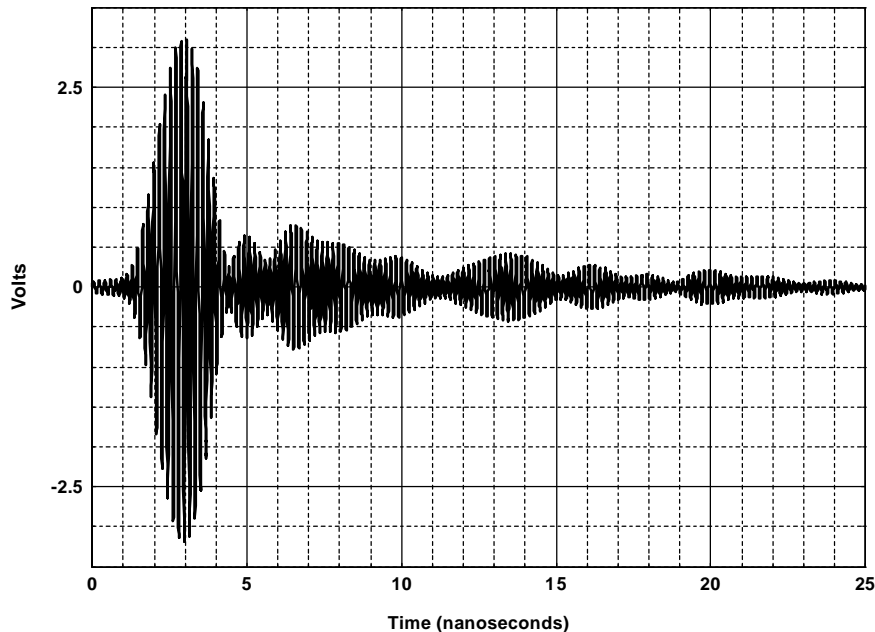


Figure 8.1. Device A full bandwidth pulse shape.

Depending on the UWB device, the full bandwidth pulse shape measurements were made on a conducted basis and/or a radiated basis at a distance of 1 meter. Conducted measurements were calibrated in dBm; radiated measurements were calibrated in voltage available at the terminals of a ridged horn or TEM horn antenna at a distance of 1 m. For the radiated measurements, the effects of the measurement antenna frequency-dependent gain and delay on the pulse shape have not been corrected, though techniques to provide a calibration in absolute field-strength are still being investigated. This process would involve performing an FFT of the uncorrected pulse, correcting the resulting spectrum with frequency-dependent antenna delay and gain factors, and performing an inverse FFT on the corrected spectrum to obtain a corrected pulse shape.

The Device A full bandwidth pulse shape in Figure 8.1 is relatively complex, involving multiple lobes and many crossings of the zero-axis. A complex waveform like this is typical of UWB signals that have been filtered with relatively high-Q resonant circuits to provide a signal limited to a well-controlled RF bandpass. Other UWB devices (e.g., Device E) may have a much simpler pulse shape with only a few zero-crossings.

8.2.3. FFT Emission Spectrum

Figure 8.2 is an example of an emission spectrum calculated via FFTs from the full-bandwidth pulse shape in the previous figure. Device A's full bandwidth pulse shape was measured in the conducted mode, so the spectrum calculated via FFTs was calibrated in peak dBm in a specific bandwidth Δf . In this case, a Δf bandwidth of 16.7 MHz was used. For large bandwidths, the calculated peak dBm will change according to a $20 \log_{10} B$ rule.

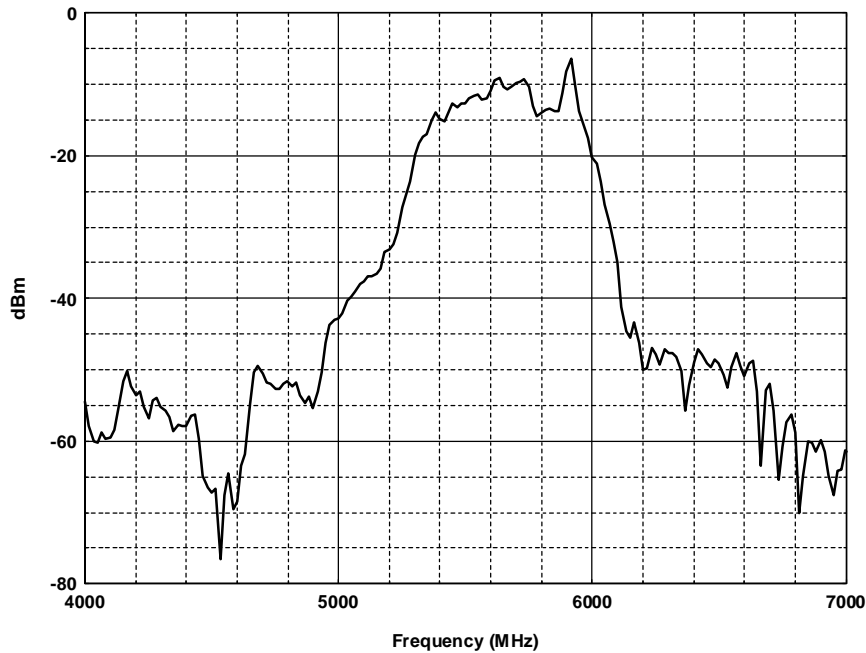


Figure 8.2. Device A conducted FFT spectrum, $\Delta f = 16.7\text{MHz}$.

Most of the UWB devices were measured in the radiated mode at a distance of 1 meter. In the radiated pulse shape measurements, the pulse shape was not corrected for the effects of the frequency-dependent receiving antenna gain. However, the spectrum calculated from the pulse shape via FFTs is corrected for antenna gain and plotted as field strength at 1 meter. The field strength values are based on peak power in a given computational bandwidth, Δf , and plotted in $\text{dB}\mu\text{V/m}$. The peak field strength can be directly compared to the spectrum analyzer measurements by using an appropriate bandwidth conversion factor (e.g., $20 \log_{10} B$ for wider bandwidths where the UWB pulses are independently resolved). The FFT is based on the

emission from a single pulse. Therefore, it contains none of the spectrum fine structure caused by a train of impulses and the associated pulse train modulation techniques.

Major objectives for FFT calculation of emission spectra include a comparison with spectrum analyzer measurements. Close agreement between FFT and measured spectra ensures confidence in the accuracy of the full-bandwidth pulse shape measurements and the adequacy of narrowband spectrum analyzer measurements in determining the RF envelope of UWB emissions. Since the Device A full bandwidth pulse shape (and the corresponding FFT spectra) was measured in the conducted mode, while the spectrum analyzer measurements in the following sections were made in the radiated mode, no direct quantitative comparison of the full bandwidth measurements and the spectrum analyzer measurements is possible. A full set of radiated measurements were made with many of the other UWB devices, however, and these show good quantitative comparison between the full bandwidth data and the spectrum analyzer data. On a qualitative basis, the Device A conducted FFT spectrum shows the same concentration of energy in the 5300-6100 MHz region shown in the radiated spectrum analyzer measurements described next.

8.2.4. Narrowband Peak Emission Spectra

Figure 8.3 contains a series of emission spectra measured at a distance of 1 m with a spectrum analyzer using a peak detector and bandwidths of 10 kHz to 3 MHz, as described in Section 6.4.2. This data is calibrated using two scales: The left-hand scale is in dBm, referenced to the antenna terminals of an imaginary antenna having a constant aperture equivalent to what a 5.9 dBi antenna would have at 1 GHz. This calibration removes the effects of a frequency-dependent receiving antenna aperture (unlike the full-bandwidth pulse measurements), leaving the dBm value unchanged at 1 GHz. The right-hand scale is in dB μ V/m at a distance of 1 m. The details of these calibrations can be found in Appendix C.

Major objectives for these measurements include development of techniques for UWB spectrum measurements using commercial off-the-shelf (COTS) equipment, investigation of the relative utility of -10-dB and -20-dB and mid-band frequency points on the UWB spectra, peak detector bandwidth correction factors, investigation of preferred spectrum measurement bandwidths for various regulatory and modeling purposes, and comparison with spectra derived by FFT processing of full bandwidth pulse shapes. Successful comparison between the FFT-derived emission spectra and spectrum analyzer measurements would strongly suggest that spectrum analyzer measurements in a narrower bandwidth are accurate and adequate for purposes of describing the overall UWB emission spectrum, along with the -10-dB and -20-dB frequency points.

If the measurement system bandwidth is sufficiently greater than the UWB device PRR, the UWB impulses are resolved in the measurement system IF as independent, non-overlapping pulses – also called “impulsive” behavior. The peak value of these pulses is expected to depend on the measurement bandwidth, B, according to a $20 \log_{10} B$ rule. This would result in approximate 10-dB differences between successively larger measurement bandwidths, when

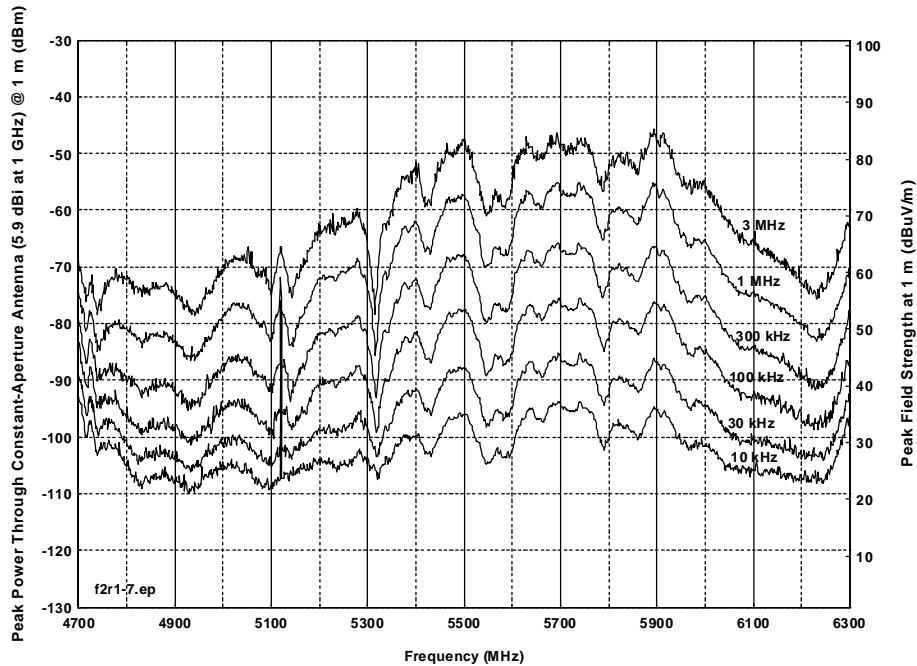


Figure 8.3. Device A measured spectra as a function of bandwidth.

those bandwidths increase in a 1, 3, 10 progression. In this example, the 10-kHz PRR of Device A causes the peak signal to appear impulsive for all measurement bandwidths greater than 10 kHz (i.e. all of the bandwidths measured in Figure 8.3).

If the measurement bandwidth is less than the UWB PRR, the UWB energy is stretched out in time in the receiver IF such that successive UWB pulses overlap, causing the appearance of a more-or-less continuous signal. Depending on the timing between successive UWB impulses, the IF signal can appear like a continuous wave (CW) signal, or Gaussian noise, or other modulations. Signals that appear noise-like are expected to follow a $10 \log_{10} B$ rule. This would result in approximate 5-dB increases between successively larger measurement bandwidths, when the bandwidths follow a 1, 3, 10 progression. Signals that have a CW appearance do not change in amplitude as the measurement bandwidth is increased. In this example, since no emission spectrum measurements were made with bandwidths less than 10 kHz, there was no opportunity to observe the behavior of signals from Device A in the noise-like or CW region.

Most of the energy in this spectrum is contained in the 5300-6100 MHz range. These spectra have numerous irregular lobes that were about 250 MHz wide, with 10-20 dB nulls between them. Detailed measurements showing UWB signal behavior as a function of higher spectrum resolution, bandwidth, and/or time, as described in the remainder of this section, were made near 5700 MHz. The measurements near 5700 MHz show an impulsive behavior (10 dB between successive measurement bandwidths). Measurements made near 4800 MHz or 6200 MHz tend to show 5-dB differences between successive bandwidths. This was probably because the UWB peak signals were not sufficiently above the measurement system noise levels near these

frequencies, and the measurements were substantially affected by system noise (5-dB difference between successive detector bandwidths).

8.2.5. Spectrum Fine Structure

The details of the spectrum fine structure are a result of the techniques used for dithering or modulating the pulse train. In general, various measurements of the detailed spectrum fine-structure were attempted for all UWB devices, but these measurements sometimes provided inconclusive results that were not included in this collection of significant measurement results. The purpose of these measurements was to gain information on PRR and modulation details so that later measurements of APDs and detector values could be understood more completely.

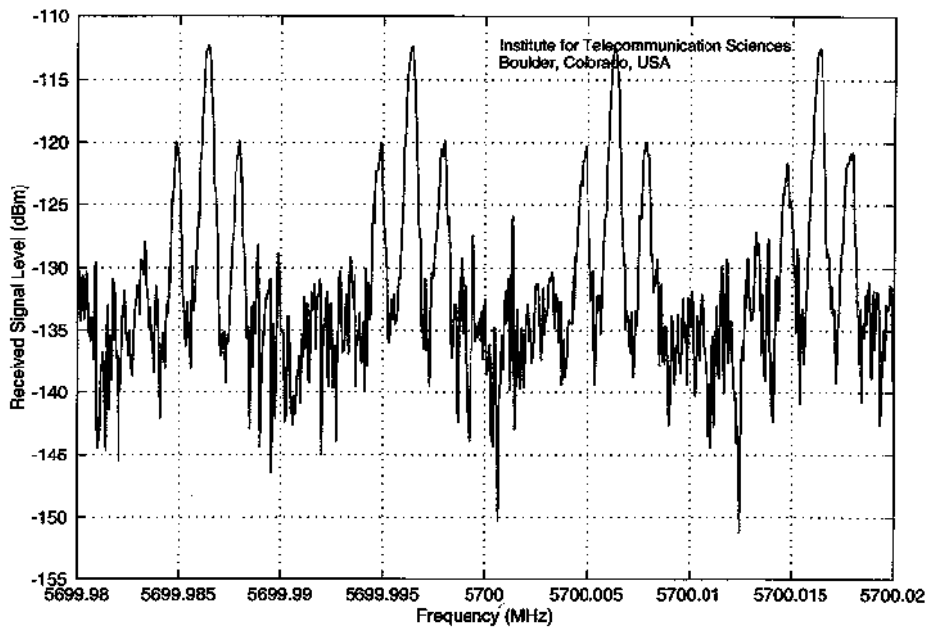


Figure 8.4. Device A spectrum fine structure (5700 MHz).

Measurements of spectrum fine-structure may reveal unexpected details like the repetition frequency of the sequence used to dither the impulse train, etc. Specifically, non-dithered pulse trains will show discrete spectral lines at harmonics of the PRR. When the basic PRR is dithered with a sequence that repeats at a certain rate, discrete spectral lines will appear separated by that rate (frequency). The relative amounts of energy in the spectral lines caused by the dither sequence, the spectral lines caused by the PRR, and the continuous spectral background are determined by the modulation and dithering details.

Device A (Figure 8.4) showed major spectral lines at a 10-kHz spacing, as expected from the 10-kHz PRR that was measured in the time domain. A closer examination showed the additional fine structure of distinct spectral lines on either side of the main lines about 1700 Hz away. The cause of these sidebands is not known.

8.2.6. Bandwidth Progression Stairstep Measurements

This measurement shows the values of peak detector readings made with a range of measurement bandwidths (100 Hz - 3 MHz). Specifically, it shows that the UWB device PRR causes impulsive behavior (10-dB steps between successive measurement bandwidths) for bandwidths greater than the PRR. For bandwidths less than the PRR this graph will show noise-like (5-dB steps between successive bandwidths), CW-like (constant values independent of bandwidth), and various other behaviors.

Figure 8.5 shows the peak signal level bandwidth progression measurements for Device A (PRR = 10 kHz), showing 10-dB spacing for bandwidths greater than 10 kHz. The apparent departure from 5-dB spacing for some of the narrower measurement bandwidths is caused by: 1) the details of the dithering technique, 2) the measurement frequency, and 3) the lower number of independent samples (which limits the ability of the peak detector to reach statistically valid peak

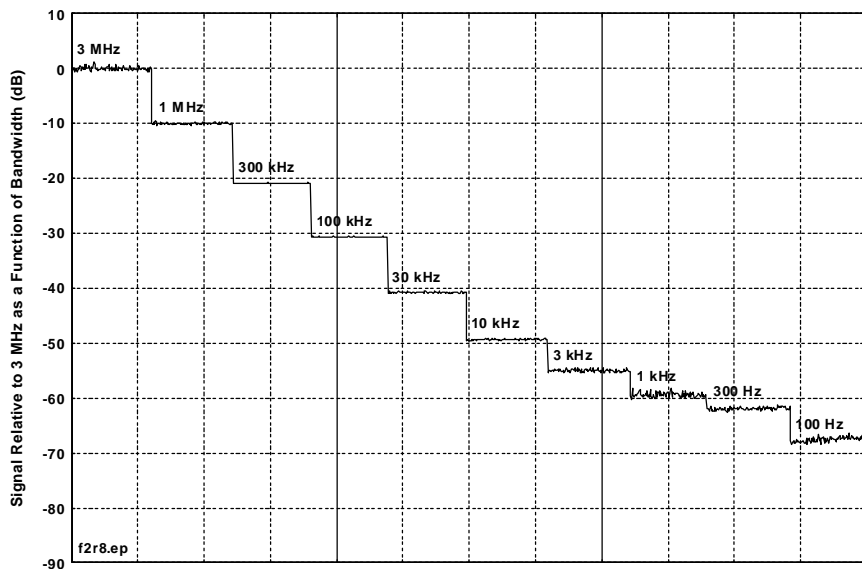


Figure 8.5. Device A, peak signal bandwidth progression stairstep .

values). This last factor is apparently not present in the Device A measurements, but it can be seen clearly in the measurements of some of the other devices (e.g. Device B, Figures 8.20 and 8.21). It is present in those cases because the rate at which independent samples occur is proportional to the measurement bandwidth, and the decreased bandwidth results in fewer independent samples during the fixed time period of these samples. This accounts for the jagged appearance of the narrowest bandwidths, where many of the time samples failed to contain any of the statistically rarer peaks that are 8-10 dB above the average values. For these cases, the 5-dB rule appears to be maintained more closely if one considers the peak value seen within the whole stair “step.” Using the whole “step” has the effect of increasing the number of independent samples for the lowest bandwidths, partially correcting the problem of too few samples.

8.2.7. Gating, PRR, and Modulation

These observations are intended to show the occurrence of patterns of pulses, as measured in the time domain at a single frequency. The purpose of these measurements was to help gain detailed information on PRR and modulation so that later measurements of APDs and detector values could be understood more completely. Depending on the features employed in a specific UWB device, these measurements could show the basic PRR (Figure 8.6), the pattern of gated pulse bursts (Figure 8.23), or the modulation method used to add dithering or data to the pulse trains (Figure 8.26). Such modulation methods could include on-off modulation of individual pulses, fixed or variable pulse delays referenced to an absolute time base, or fixed or variable pulse delays referenced to the preceding pulse. These measurements can be gathered under a wide range of bandwidths, time scales, and detector types, as needed to best show the details of the significant features.

Figure 8.6 shows the appearance of the Device B as a function of time, as seen using a wideband RF detector with logarithmic compression. This figure shows a 100-kHz PRR gated pulse train, without apparent dithering or other modulation.

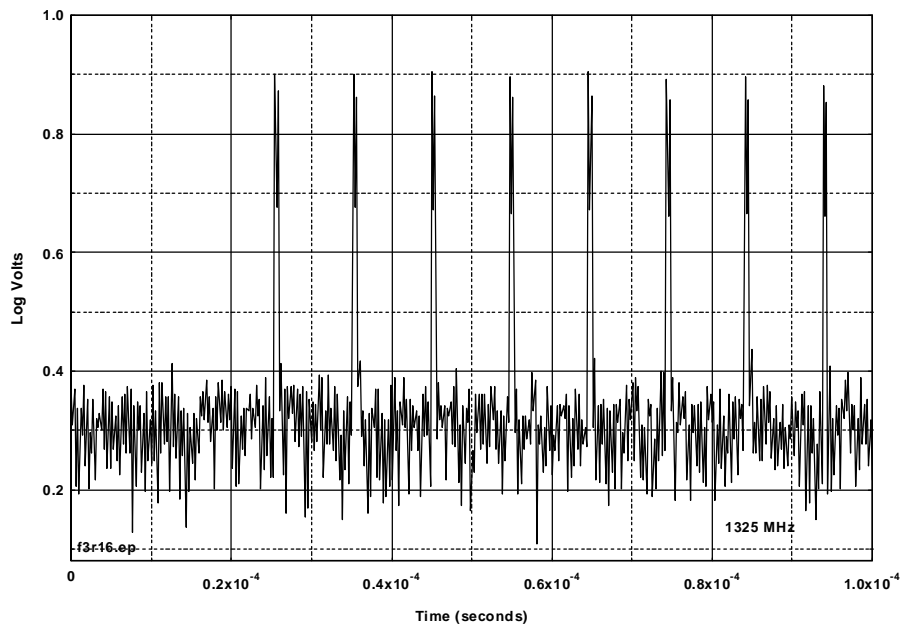


Figure 8.6. Device B, pulse train PRR, 16 kBit/second mode, external detector.

In addition to dithering (used to make UWB emission spectra look more noise-like) and modulation (employed to provide for transmission of data), some UWB systems also employ gating. A gated system employs a programmed set of periods where the UWB transmitter is turned off or on for a period of many UWB pulses. For example, a UWB system might transmit a gated burst of data lasting 10 ms, followed by a 40-ms period where no pulses are transmitted.

These so-called “gated” modes are different from data encoding techniques, where individual pulses are turned off or on to encode a digital message.

8.2.8. Amplitude Probability Distribution (APD)

The APD contains information on the percentage of time the envelope of UWB signals in a specific IF bandwidth exceeds various amplitudes. A more complete description of APDs is included in Appendix A. Figure 8.7 contains APDs from Device D, 1-MHz PRR, 100% gating (i.e., transmitting continuously). These APDs were measured in bandwidths between 10 kHz and 20 MHz at a single center frequency near the frequency of maximum UWB spectral power. With some devices, two sets of APDs were measured to distinguish between different signal fine structures seen at different frequencies. Some UWB devices measured earlier in the measurement program did not include the 10-MHz and 20-MHz bandwidth measurements, as this capability was not yet available to us.

Since the APD will change substantially as a function of measurement bandwidth (or in victim receivers having various bandwidths), the graph contains a family of APDs measured in bandwidths between 10 kHz and 3 MHz, and sometimes including 10-MHz and 20-MHz bandwidths. The APD provides a conceptual technique for understanding how various UWB signals will appear within victim receivers of various bandwidths. In particular, since the raw bit error rate of a victim receiver is closely related to the probability that the interfering UWB signal will exceed the amplitude of the desired signal, the APD provides a tool to relate UWB characteristics to the interference caused to various victim systems. (Note that many modern systems employ a variety of error correction techniques that are intended to correct most raw bit errors, so the number of errors presented to the system user may be related to the APD in more complex ways.)

The APD graph is plotted in power (dBm) versus the percentage of time (or probability) that the signal envelope will exceed a specified level. The percentage-of-time scale is weighted as $0.5 \log_{10}(-\ln P(A>a))$, as described in Appendix A. This particular weighting function has two important consequences. First, the envelope of Gaussian noise (including receiver noise) plots as a straight line, making it easy to recognize when UWB signals act in a non-Gaussian manner. Second, these APD graphs never reach 0% or 100%, but only approach these percentages. This reflects the real world circumstance that the maximum and minimum peak amplitudes of many phenomena (including Gaussian noise) are dependent on the total number of independent measurements included in the sample.

In the APD graph, the individual APDs are labeled by IF measurement bandwidth. The amplitude (power) scale is in dBm, referred to the output terminals of the measurement antenna, which was located 1 m from the UWB source. The gain of the ridged-horn measurement antenna was between 5 dBi and 10 dBi, depending on the measurement frequency. Although the APD calibration could have been converted to field strength, the primary object of the APD

measurements and analysis was to show the relative behavior of UWB signals as a function of measurement bandwidth (where absolute field strength calibration was less important).

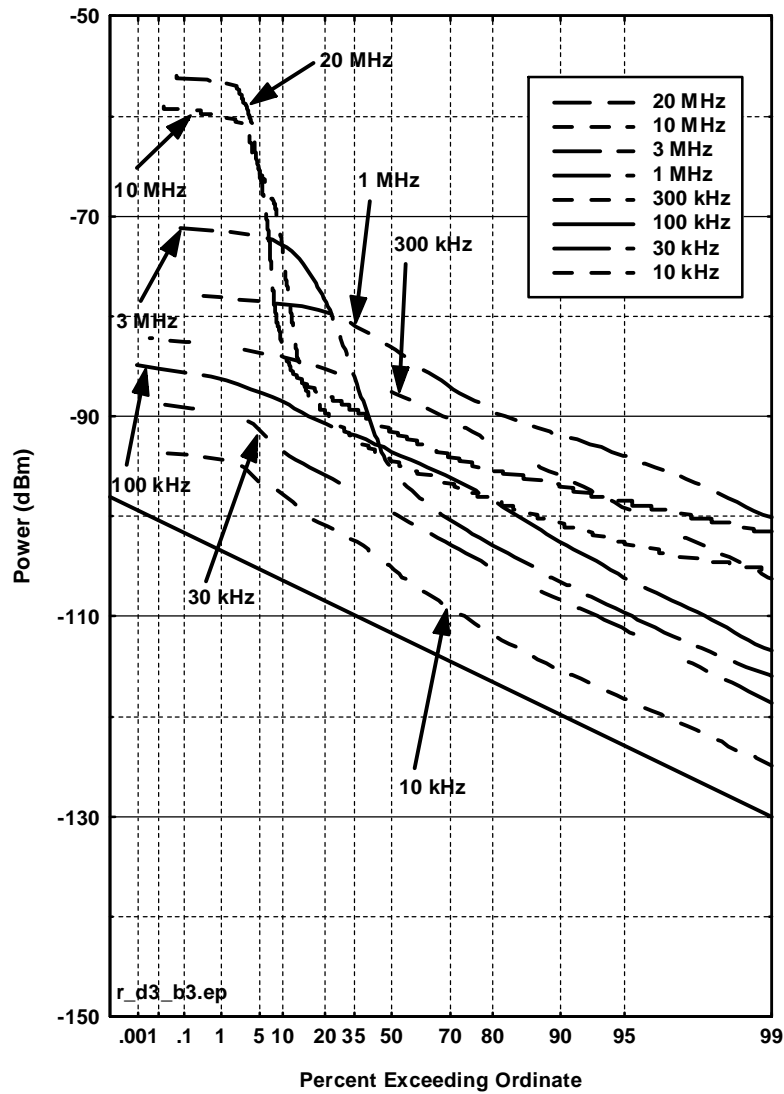


Figure 8.7 Device D APDs, 1-MHz PRR, 100% gating.

Most APDs show two distinct patterns, depending on the relationship of the measurement bandwidth to the PRR. For measurement bandwidths greater than the PRR (bandwidths of 3 MHz and above for Device D, PRR = 1 MHz), the UWB signals look impulsive. This means that the individual UWB RF impulses are converted to independent pulses within the receiver IF bandwidth. The peak amplitude of these IF pulses varies as $20 \log_{10} B$, and the duration of these pulses is approximately $1/B$. For example, in the 10-MHz bandwidth, each pulse will last approximately 0.1 μ s. With a PRR of 1 MHz, the total duration of these pulses adds up to a total of 0.1 s each second. This is a total pulse duration equal to about 10% of the total time, matching the approximate 10% “plateau” on the 10-MHz APD in Figure 8.7.

The peak amplitude of the plateau is expected to vary according to a $20 \log_{10} B$ rule for independent pulses. Thus, the 20-MHz APD should have a peak value 16.5 dB greater than the 3-MHz APD – very close to the difference in Figure 8.7.

As shown in the graph, the Device D pulse was present in the 20-MHz bandwidth about 5% of the total time. During the 95% of the time that the Device D pulse was not present in the measurement receiver, the only “signal” present in the measurement receiver was receiver system Gaussian noise. Thus, the remainder of the APD (after the impulsive signals have been subtracted) is only system noise. In the example, the 20-MHz APD tends to match a straight line drawn on the graph corresponding to Gaussian noise over the percentage ranges between about 20% and 80%. This straight line corresponds to a 20-MHz receiver bandwidth with a noise figure of 10 dB. The APD of system noise corresponding to other bandwidths and noise figures would be represented by a straight line with an identical slope, but offset vertically and intercepting the 37% value at $\text{Noise (dBm)} = \text{NF} + 10 \log_{10} B(\text{Hz}) - 174$, where NF is the measurement system noise figure in dB.

The departure of the measured APDs from the expected Gaussian noise straight line (the 80-99% range on the 20-MHz APD, and various amounts on other curves) is not completely resolved, but it is probably due to insufficient video bandwidth in the measurement system that was assembled to make the 10-MHz and 20-MHz bandwidth measurements. As expected, the departure-from-ideal-response was greater for the wider bandwidths.

Within measurement bandwidths equal to or less than the UWB PRR (1-MHz and less, in this example), the UWB energy does not appear as independent pulses. In this “non-impulsive” mode, the energy from successive UWB pulses is sufficiently stretched out in time by the IF bandwidth filter that the “pulses” overlap. Depending on the timing between pulses, the overlapping pulses can constructively or destructively interfere in the receiver IF bandwidth. This process can produce various results, including a series of discrete spectral lines at the harmonics of a uniform undithered PRR, or a continuum of energy resembling Gaussian noise for modulated or dithered UWB pulse trains. The use of a repeated binary sequence to dither the pulse train can produce discrete close-spaced spectral lines at frequencies related to the repetition rate for the whole sequence.

Although some dithering or modulation techniques may produce signals that appear like Gaussian noise in narrow bandwidths, this apparent Gaussian noise is different in origin from the Gaussian noise that is present in the wider bandwidth impulsive modes and in gated modes. In the narrowband mode (bandwidths less than the PRR) the energy from ungated UWB impulses is continually present in a narrow IF bandwidth, and the measured signal (often a signal with Gaussian characteristics) comes from the UWB energy. In wideband and gated modes, there are time intervals where no UWB energy is present, and measurement system (Gaussian) noise appears whenever the UWB energy is absent. Therefore, although the APDs measured in these two cases may both appear like Gaussian noise, it is important to note that for gated signals or wide measurement bandwidths the low amplitude Gaussian portion of the APD is not caused by

the UWB signal. In the case of the Device D example, the amplitude of the Gaussian noise in the 30-kHz APD is about 17 dB higher than would have been calculated on the basis of system noise figure and bandwidth.

8.2.9. Detector Summary

While the complete APD data set may give good insights on how specific UWB devices will interact with specific victim receivers, a specification for computing a single numerical value from any APD may be desirable for comparing UWB emissions with regulatory limits. APDs can be processed to give numerical values for detector functions (called “statistics” in Appendix A) like peak, RMS, average voltage, average logarithm, median, etc. The specific intent of this section is to explain the numeric values produced by various detectors and measurement bandwidths, based on the particular characteristics of UWB signals. These results are intended to give information on which detector functions and bandwidths are most suited for specifying Part 15 limits, rather than to suggest specific numerical values for these limits.

Since the APD contains only first-order statistics, presumably any detector function that can be derived from first-order statistics can be computed from the APD. The detector summary analysis computes the following detector values from APDs measured in various bandwidths: peak, RMS, average voltage, and average logarithm. In some EMI receivers and newer spectrum analyzers these statistics are made available by hardware detectors or real-time digitizer/signal processors designed to process the IF signal in comparable ways. The quasi-peak detectors specified by the FCC for most Part 15 measurements below 1 GHz cannot be computed from the APD, because quasi-peak measurements are a function of second-order statistics, as well as first-order statistics.

8.2.10. FCC Proposed Part 15 Measurement Procedures

The FCC suggested in the UWB NPRM that UWB devices be measured according to the existing Part 15.35 (b) measurement techniques referred to in Part 15.209. These measurement techniques include quasi-peak detectors for frequencies below 1 GHz and a pair of measurements (average and peak) for frequencies above 1 GHz. For frequencies above 1 GHz, the FCC specifies in 15.35 (b) that measurements shall be made using an “average detector function.” It also states that a maximum peak UWB value should be no more than 20 dB above the average limits, and that (unless otherwise specified) measurements should be made with a minimum bandwidth of 1 MHz. Based on this text, we believe that the FCC has described a Part 15 average detector function corresponding to the average voltage value computed from the 1-MHz APD.

However, the FCC has proposed in their NPRM (Question #50) that Part 15 average measurements be made with a spectrum analyzer using 1-MHz bandwidth, video filtering (between 10-kHz and 10-Hz bandwidth) and a peak detector. No guidance is given in the NPRM

concerning whether logarithmic or linear IF compression is to be used.² It is likely that the use of a logarithmic IF amplifier would give a result very similar to the average logarithm value computed from the 1-MHz APD. If a linear IF were used instead of a logarithmic IF, the result should be very similar to the average voltage value computed from the 1-MHz APD. To confirm this possibility, we also performed an independent measurement that followed the FCC procedures exactly, using a 1-MHz bandwidth, logarithmic IF mode, video filtering, and sample detector. The function of the FCC peak detector is duplicated by manually reading the highest value from the resulting graph. This modified procedure makes it possible to understand the role of sufficient lowpass video filtering in the suggested FCC measurement. This result is labeled "FCC Part 15" and represented by a hollow square in the detector summary graphs.

Detector functions corresponding to peak, RMS, average voltage, and average logarithm have been computed from the APDs measured in each bandwidth and plotted at the corresponding bandwidth for Device D in Figure 8.8. Details on this computation are included in the discussion of APDs in Appendix A. These four detector functions tend to emphasize particular parts of the APD. The peak detector looks only at the single highest measurement value, ignoring all other measurement values. The RMS detector performs an integration of average power. Because power is related to "voltage-squared," the effect of the higher amplitudes in the APD is enhanced. The average voltage detector tends to be affected more equally by the whole range of values. The average logarithm detector gives greatest weight to the lower values. The detectors are normalized to give the same value for a CW signal.

Some common "rules-of-thumb" for these detectors (which should be tested against the detector values actually obtained) include:

1. For Gaussian noise, the peak detector value is typically 8-11 dB greater than the RMS value (depending on the number of samples), the average voltage is 1 dB less than the RMS value, and the average logarithm is 2.5 dB less than the RMS value. The RMS value is exceeded 37% of the time.
2. For non-overlapping pulses, the peak value varies as $20 \log_{10} B$.
3. The RMS value varies as $10 \log_{10} B$
4. Peak \$ RMS \$ average voltage \$ average logarithm.

Figure 8.8 shows the detector summary graph for Device D, 1-MHz PRR, 100% gating. Dashed lines have been drawn on the graph, corresponding to $10 \log_{10} B$ and $20 \log_{10} B$ slopes. These lines are intended as graphical aids, not as suggested conclusions.

²In a separate communique related to the NTIA UWB test plan, the FCC indicated that the intention was to employ the spectrum analyzer in the logarithmic IF mode.

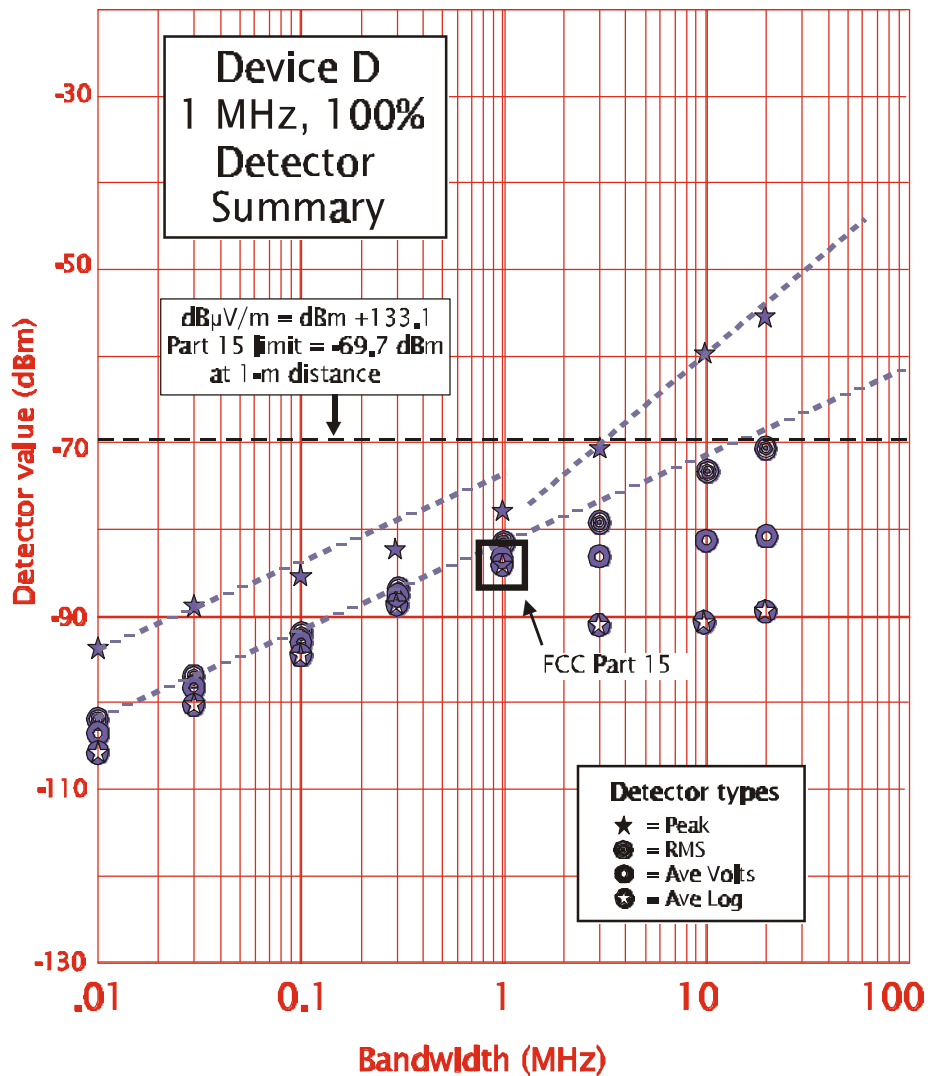


Figure 8.8. Device D detector summary, 1-MHz PRR, 100% gating.

The detector summary shows two major regions: the impulsive region ($B \gg \text{PRR}$) and the noise-like region ($B \ll \text{PRR}$). In the noise-like region, the values for the RMS, average voltage, and average log detectors are closely spaced (2.5 dB theoretical difference between average log and RMS for Gaussian noise). The peak reading is about 8 dB above the RMS (the peak value is theoretically 8-11 dB above the RMS value for Gaussian noise). The values for all detectors change according to a $10 \log_{10} B$ trend. The similarity between the Device D detector readings and the corresponding readings that would have been theoretically produced by Gaussian noise suggest that the Device D signal dithering was selected to make it look similar to Gaussian noise.

A completely different pattern of detector function values is found in the impulsive region ($B \gg \text{PRR}$). There is a much wider divergence between various detector values at any single bandwidth, and this divergence becomes greater as the bandwidth increases. The peak values follow a $20 \log_{10} B$ trend line, and the RMS values follow a $10 \log_{10} B$ trend line. The value of the average voltage and average log detectors drop substantially when the wider bandwidths allow low amplitudes associated with measurement system noise to be seen between the duration of UWB impulses. Since the average log value emphasizes the lowest amplitude signals, the average logarithm value is most dramatically affected when the IF output drops to the measurement system noise level between impulses. The difference between peak values and average logarithm values is as much as 35 dB for the 20-MHz bandwidth. These relatively large differences between detector values suggest that the detector functions used in measuring Part 15 regulatory limits must be specified unambiguously.

The smallest differences between the various detector functions is often seen when $B = \text{PRR}$. In this example, there is only a 6-dB difference between average logarithm and peak values for the 1-MHz values.

The FCC-proposed Part 15 measurement procedure using a spectrum analyzer with 1-MHz bandwidth, logarithmic IF, video filtering, and peak detection was used to make a direct measurement of the Device D signal. This measurement produced a value of about -84 dBm, which was essentially identical to the average logarithm detector value computed from the 1-MHz bandwidth APD.

In addition to the dBm scale on the detector summary graphs, a level has been marked with a horizontal dashed line. This level corresponds to the FCC Part 15 limits from 15.209, which is specified as 500 $\mu\text{V/m}$ at a distance of 3 meters. Since all of the measurements in this section of the report were measured at a distance of 1 meter, the FCC limit has been adjusted for a 1-m distance and the gain of the antenna used for the measurement. More details on this conversion can be found in Appendix C.

8.3 Measured Data Summaries for Devices

The following sections contain compilations of measured data from UWB devices A-E and an electric drill. Additional measured data on each device is contained in a corresponding separate section in Appendix D.

8.3.1 Summary of Device A Measurements

Device description. Device A uses a 10-kHz PRR, apparently not gated, dithered, or modulated. ITS had no information on the operational aspects of this device, and testing proceeded on the assumption that the on-off switch was the only significant test variable.

Full bandwidth pulse shape. Figure 8.9 shows a complex pulse shape with multiple lobes, probably caused by a multipole sharp-cutoff RF filter giving a tightly-defined UWB spectrum.

FFT emission spectrum. Figure 8.10 shows most UWB energy is in the 5100-6100 MHz band.

Narrowband peak emission spectra. Spectrum analyzer measurements (Figure 8.11) show most energy in the 5100-6100 MHz range. This spectra had 5-6 irregular lobes about 250 MHz wide, with 10-20 dB nulls between them.

Spectrum fine-structure. Figure 8-12 shows details near 5700 MHz reflecting the 10-kHz PRR of Device A .

Bandwidth progression staircase. Figure 8-13 clearly shows 10-dB steps for bandwidths greater than the 10-kHz PRR (impulsive behavior) and 5-dB steps (noise-like behavior) for bandwidths less than 10 KHz .

APDs. Figure 8-14 shows impulsive behavior for all measurement bandwidths greater than 10 kHz. However, although the peak values followed a $20 \log_{10} B$ trend line for the narrower bandwidths, the 1-MHz and 3-MHz peak values (Figure 8.15) were appreciably lower than the trend line (8 dB lower at the 3-MHz bandwidth). This 8-dB difference was traced to a deficient component in the spectrum analyzer, which was found to provide insufficient spectrum analyzer video bandwidth and was replaced by the manufacturer. Unfortunately, Device A had already been returned to its owner when the repaired spectrum analyzer became available. It should probably be assumed that a re-measurement of Device A would have placed the 1-MHz and 3-MHz readings on the proper trend lines.

Detector summary. We note in Figure 8-15 that the detector values are within 8 dB of each other in the 10-kHz measurement bandwidth, and they diverge rapidly as the bandwidth is increased. The difference between peak and average logarithm is as much 40 dB for the 3-MHz bandwidth (presumably, this difference would have been 8 dB greater – a 48-dB difference – if the spectrum analyzer had been working properly during these measurements).

FCC Part 15 measurement. The FCC-recommended Part 15 measurement procedure (1-MHz bandwidth, logarithmic IF, video filtering, and peak detection) produced a value of -112 dBm with a 300 Hz video bandwidth (300 Hz was the minimum video bandwidth for the spectrum analyzer when used with 1-MHz resolution bandwidth). This matches the -112 dBm average logarithm detector value in Figure 8-15 computed from the 1-MHz bandwidth APD.

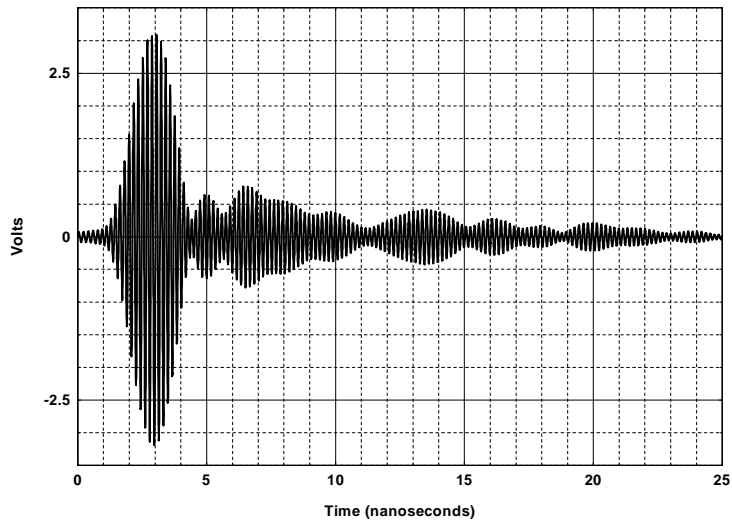


Figure 8.9. Device A full bandwidth pulse shape.

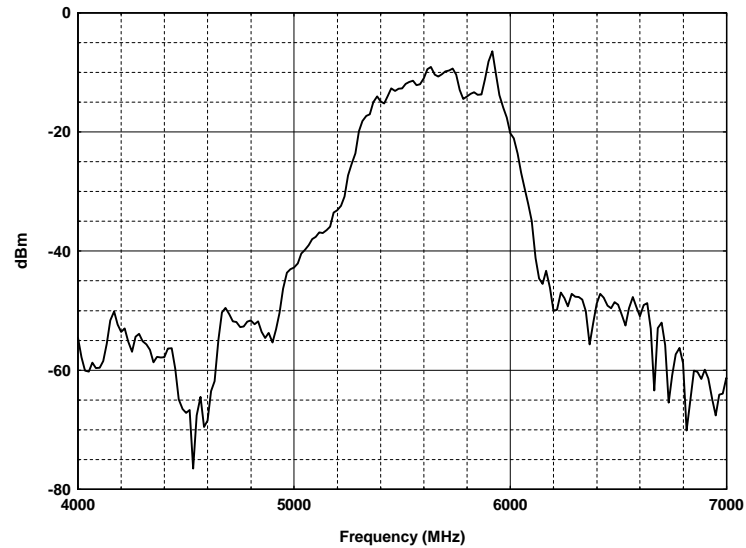


Figure 8.10. Device A, conducted power spectrum, $f = 16.67$ MHz.

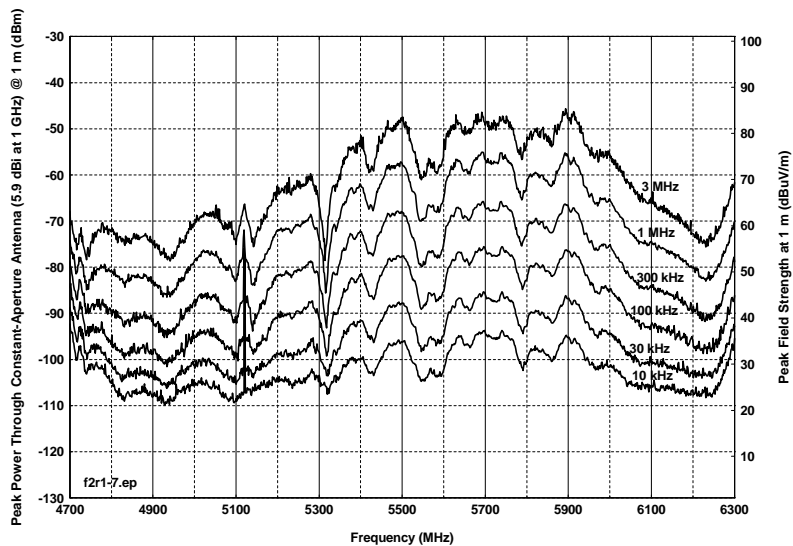


Figure 8.11. Device A spectra as a function of measurement bandwidth.

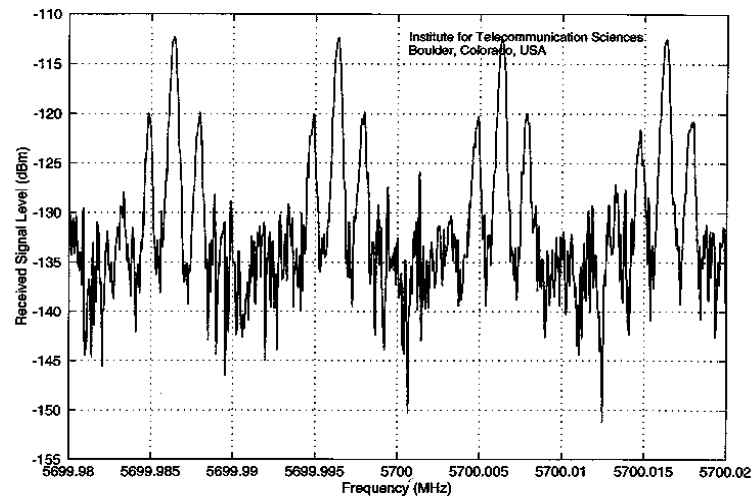


Figure 8.12. Device A spectrum fine structure.

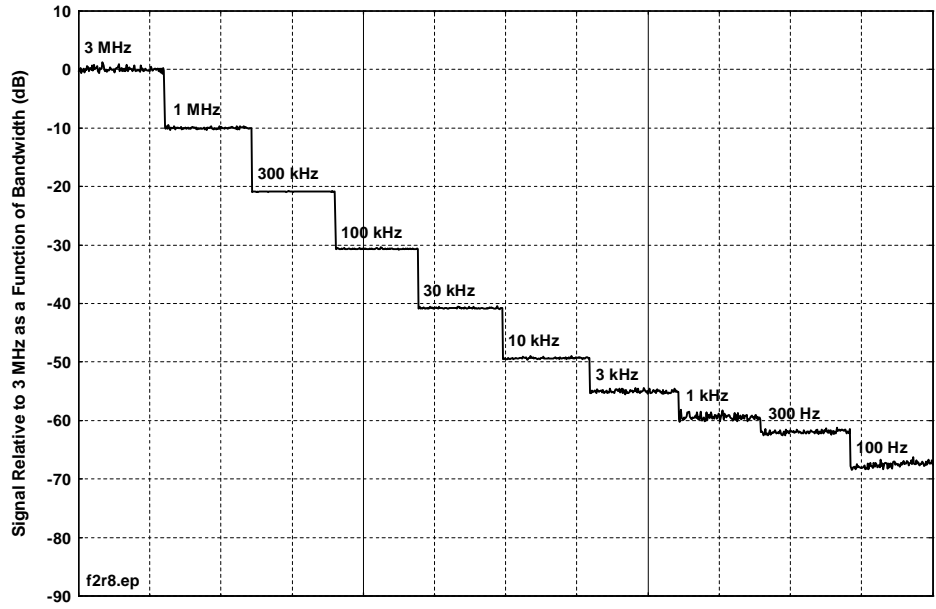


Figure 8.13. Device A peak amplitude as a function of bandwidth.

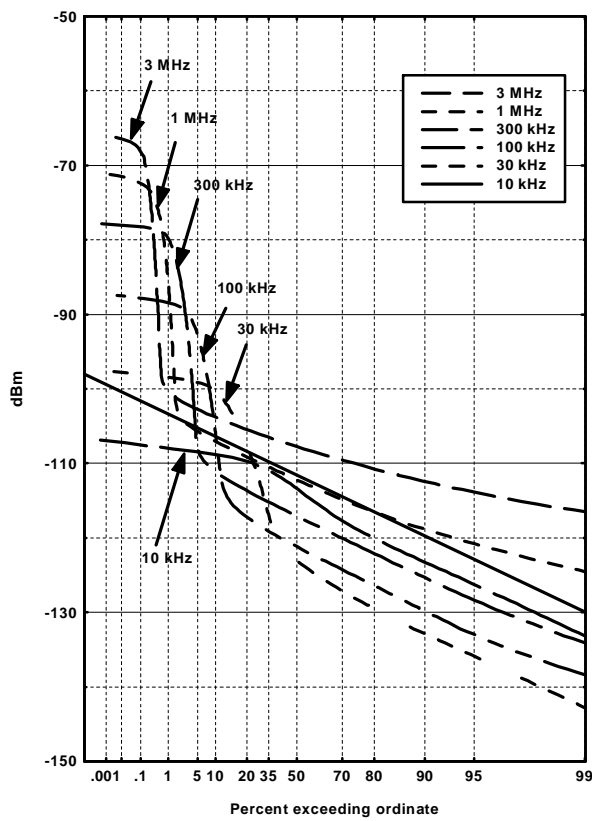


Figure 8.14. Device A APDs.

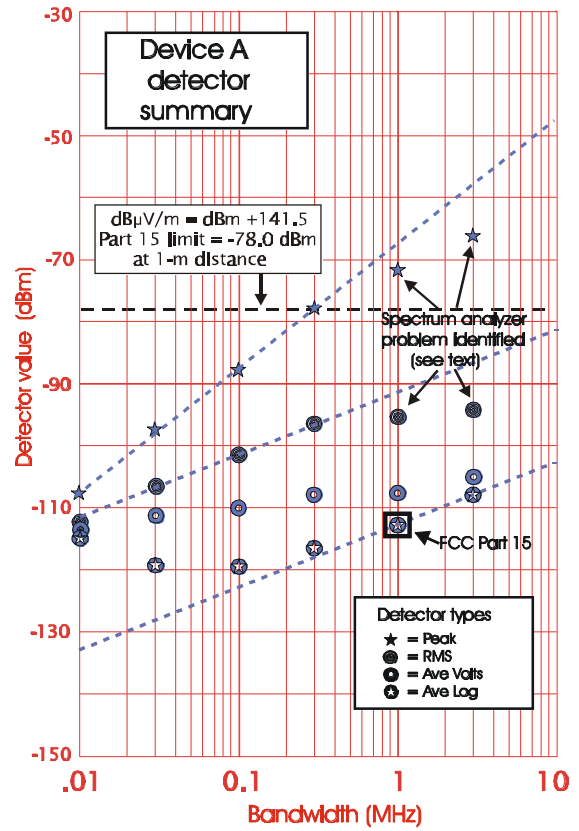


Figure 8.15. Device A detector summary.

8.3.2 Summary of Device B Measurements

Device description. Device B operates in four data rate modes, ranging between 16 kb/s and 128 kb/s. Any of these data rates can be used to support a two-way voice circuit or a two-way data circuit. ITS measured the device in its 16-kb/s and 128-kb/s voice modes, but did not measure the intermediate 32-kb/s and 64-kb/s modes.

The 16-kb/s mode provides an average user data rate of 16 kb/s, using a transmitted signal of about 100 K impulses per second, which is gated on for 8.8 ms and gated off for 35.2 ms (44 ms total cycle time). During the 8.8 ms when the signal is gated on, the data stream is modulated on the train of impulses by deleting selected pulses (on-off keying). Corresponding gating and PRR values for the other modes can be found in Table 8.1.

Table 8.1. Burst and PRR Timing for Various Data Rates

Data Rate (kb/s)	Burst length (on time, ms)	Burst Repetition time (ms)	Burst duty cycle (gating)	Pulse repetition rate (PRR)
16	8.8	44	20%	100 kHz
32	4.4	22	20%	200 kHz
64	2.2	11	20%	400 kHz
128	2.2	5.5	40%	400 kHz

Full bandwidth pulse shape. Device B emission spectrum is tightly filtered to limit it to a 500 MHz-wide bandwidth. This filtering produces relatively complex and extended pulse shapes, lasting up to 30-40 ns (Figure 8.16).

FFT emission spectrum. The FFT-derived spectrum (Figure 8.17) shows a sharply-defined 500-MHz RF bandwidth. The peak signal in the FFT-derived spectrum is 116 dB μ V/m in a bandwidth, Δf , equal to 20 MHz.

Narrowband peak emission spectra. Figures 8.18 and 8.19 show a sharply-defined bandwidth between 1250 and 1800 MHz, with 5-6 ripples of 5-10 dB depth across the passband. The peak signal measured with a spectrum analyzer in a 3-MHz bandwidth (Figures 8.1 or 8.19) is approximately 100 dB μ V/m. Since the UWB signal for Device B is impulsive at bandwidths greater than the PRR (maximum PRR = 400 kHz) a $20 \log_{10} B_1/B_2$ correction factor is needed to convert the 3-MHz bandwidth data to 20-MHz data. This correction factor equals 16.5 dB. This converts the 3-MHz bandwidth value measured by the spectrum analyzer to the corresponding 20-MHz bandwidth value of 116.5 dB μ V/m, which compares closely with the FFT-computed value of 116 dB μ V/m.

Bandwidth progression staircase. The stair step bandwidth progression figures (Figures 8.20 and 8.21) suggest that Device B produces signals that appear noise-like for measurement bandwidths less than the 100-kHz or 400-kHz PRR's associated with the respective 16-kb/s and 128-kb/s modes, made at 1325 MHz and 1500 MHz respectively.

Gating, PRR, and modulation. Figures 8.22 and 8.23 show the 20% and 40% gating duty cycles for the 16-kb/s and 128-kb/s modes, respectively. Figures 8.24 and 8.25 show the basic PRRs for the 16-kb/s and 128-kb/s modes, respectively. Figure 8.26 shows an example of a missing pulse, caused by the on-off pulse modulation of the Device B data stream.

APDs. Both APDs (Figures 8.28 and 8.29) were measured at 1545 MHz. These APDs were inadvertently measured using video filtering equal to the resolution bandwidth, which prevented the low-amplitude portion of the APD from reaching minimum values. This effect is believed to have prevented this portion of the APDs from following the expected straight line. This problem was recognized and corrected in subsequent APD measurements for other devices. The very steep sides on the "plateau" at 20% and 40% respectively for the 16-kb/s and 128-kb/s modes reflect the respective 20% and 40% gating modes.

Detector summaries. The detector summaries (Figures 8.30 and 8.31) show approximately a 30-dB difference between peak and average logarithm and a 20-dB difference between average logarithm and RMS values for the narrower bandwidths, caused mainly by the gating modes. During the gated-off period, system noise is the only signal contributing to the APD. Since the average logarithm value is affected most by low amplitude, high-percentage signals, measurement system noise has a strong effect on the average logarithm value of gated signals.

The peak value follows a $10 \log_{10} B$ trend line (like Gaussian noise) for bandwidths less than the PRR and a $20 \log_{10} B$ trend (like an impulse) for bandwidths greater than the PRR. Peak measurements are identical for both 3-MHz bandwidth APDs, where impulses are non-overlapping. For the lower bandwidths where the signal acts like Gaussian noise, peak measurements for each PRR differ by about 6 dB, which would be expected from the 4:1 ratio in the number of pulses/s (not counting the percentage gating ratio).

The RMS values follow a $10 \log_{10} B$ line for all bandwidths. The best-fit trend lines for the two modes are about 8 dB apart. A difference of 9 dB would have been expected, based on the 8:1 ratio in the total number of impulses (including the effect of the 2:1 change in gating ratio).

FCC Part 15 measurement. A measurement similar to the Part 15 measurement (except using a 3-MHz bandwidth) was done at 1650 MHz, 128 kb/s mode with logarithmic IF, 10-Hz video bandwidth, and sample detection (Figure 8.27). This gave an maximum measurement of about -74.5 dBm, with less than 1-dB time ripple caused by the 5.5 ms gating cycle. Compensating for the gain of the 19 dB preamplifier, the "Part 15-like" value was -93.5 dBm, which is within 2 dB of the average logarithm computed from the 3-MHz APD. No Part 15 measurements were made at 1-MHz bandwidth or using the 16-kb/s mode.

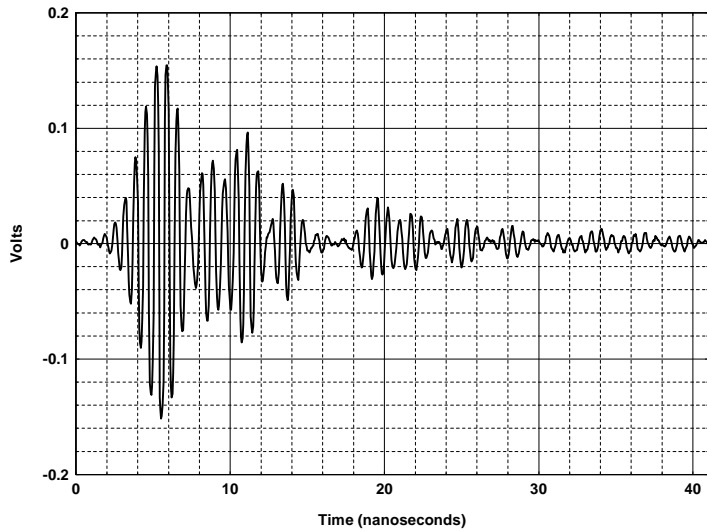


Figure 8.16. Device B full bandwidth pulse shape.

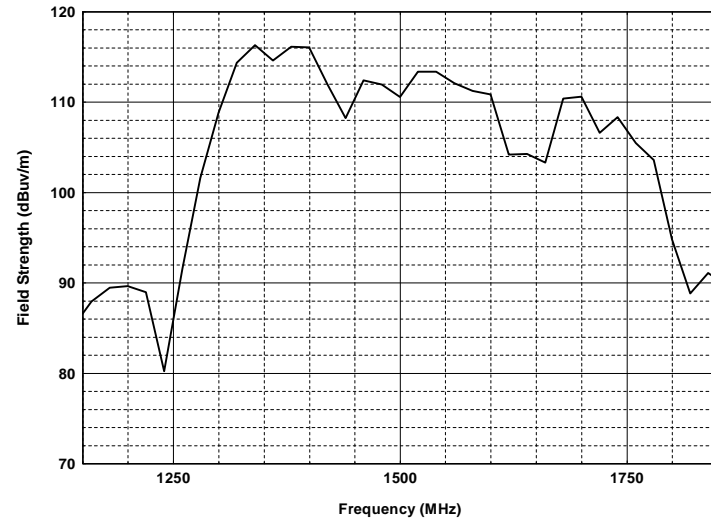


Figure 8.17. Device B, radiated peak field strength at 1 m, $f = 20$ MHz.

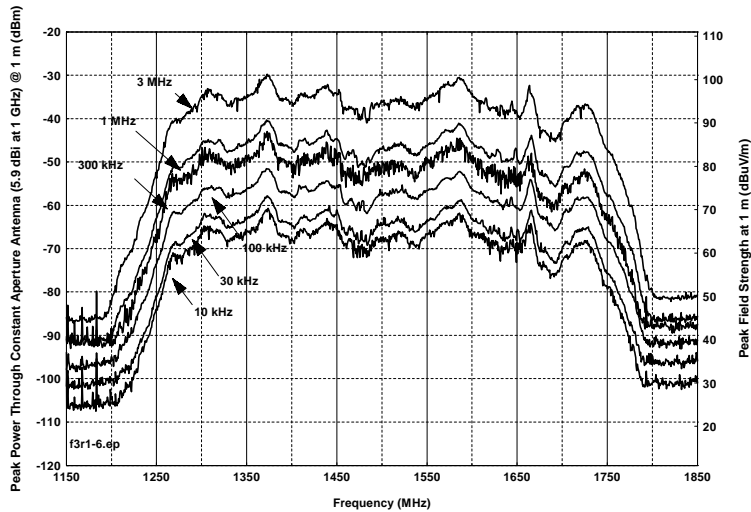


Figure 8.18. Device B, spectra as a function of bandwidth, 16-kb/s voice mode.

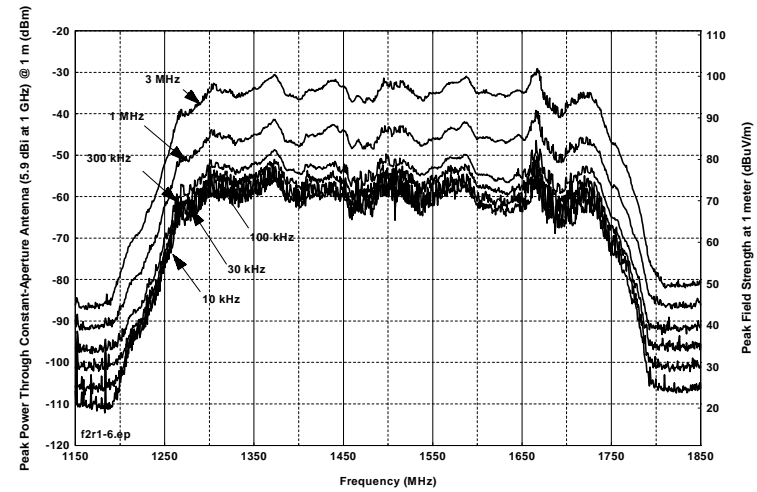


Figure 8-19. Device B, spectra as a function of bandwidth, 128-kb/s voice mode.

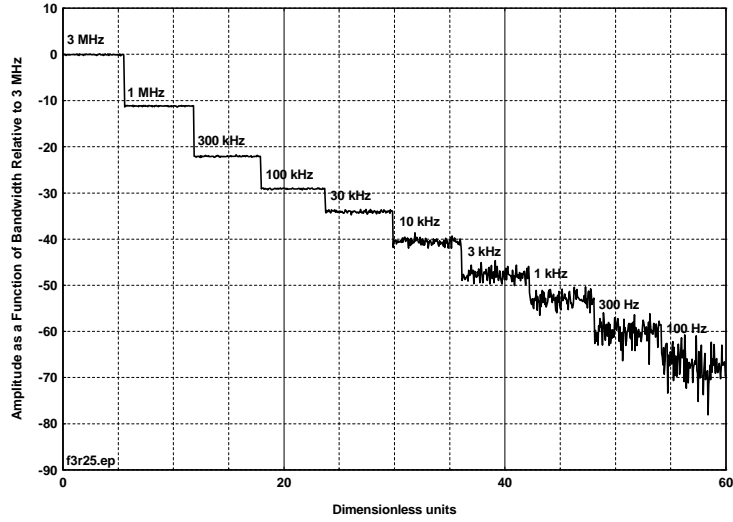


Figure 8.20. Device B, 16-kb/s voice mode, bandwidth progression staircase.

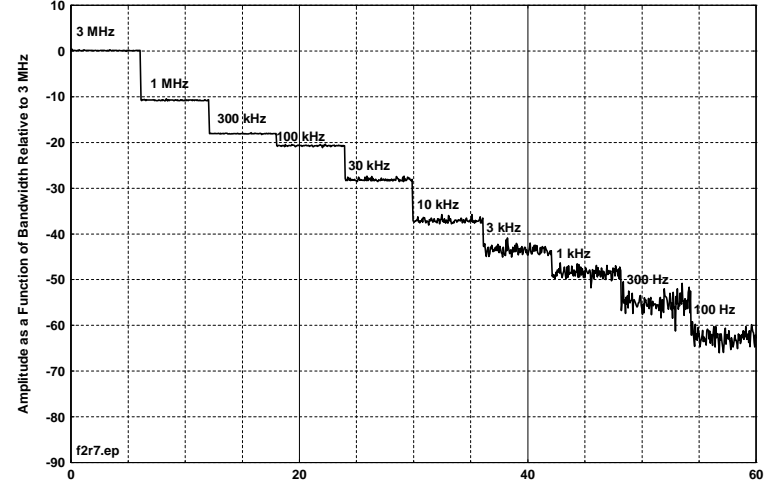


Figure 8.21. Device B, 128-kb/s voice mode, bandwidth progression staircase.

8-22

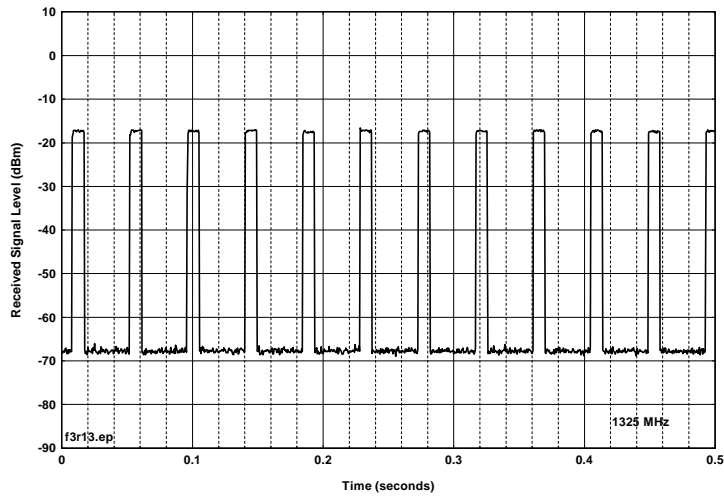


Figure 8.22. Device B, 16-kb/s mode, 3-MHz IF bandwidth, positive peak detector.

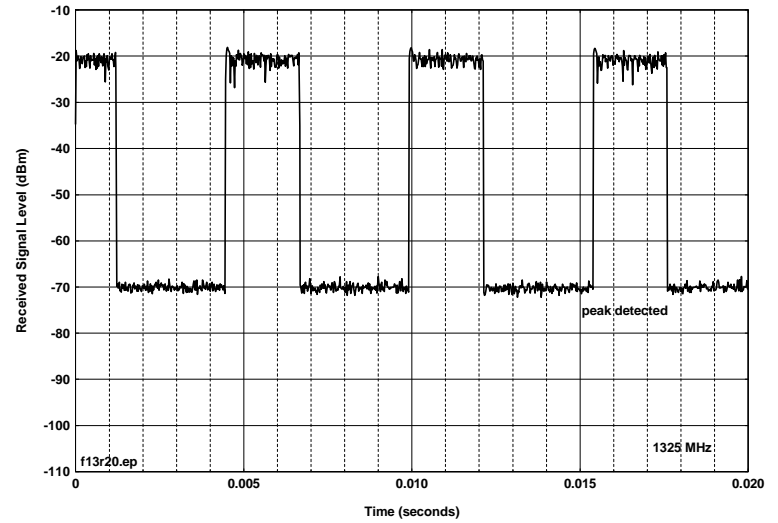


Figure 8.23. Device B, 128-kb/s mode, 3-MHz IF bandwidth.

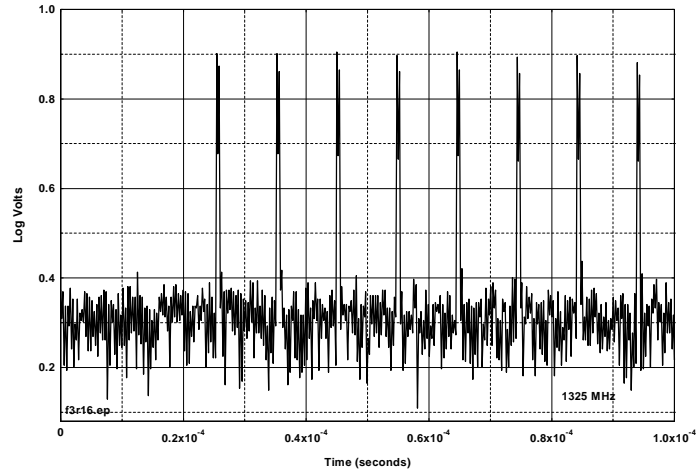


Figure 8.24. Device B PRR waveform, 16-kb/s mode, external detector.

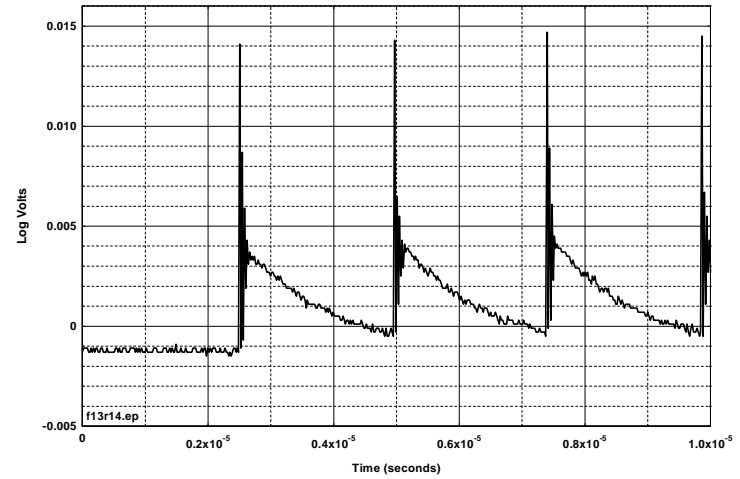


Figure 8.25. Device B PRR waveform, 128-kb/s mode, external detector.

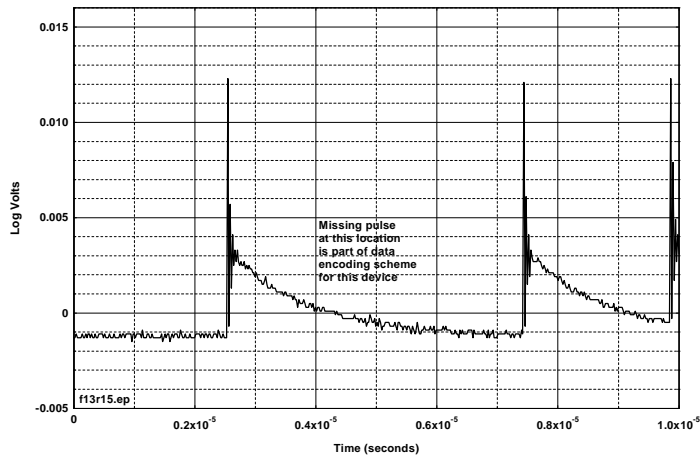


Figure 8.26. Device B, waveform showing on-off modulation, 128-kb/s mode.

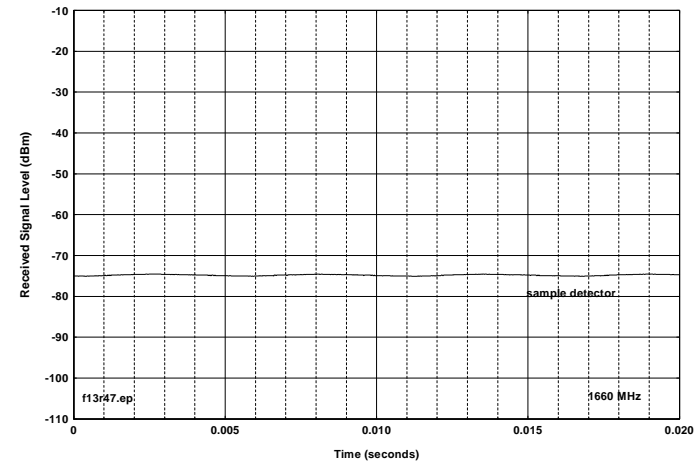


Figure 8.27. Device B, 128-kBit/second mode, 3 MHz BW, 10-Hz video (Part 15-like).

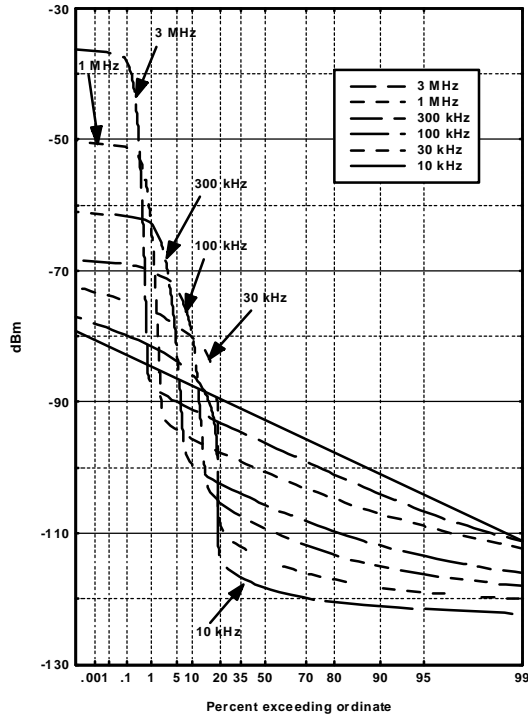


Figure 8.28. Device B APDs, 16 kb/s.

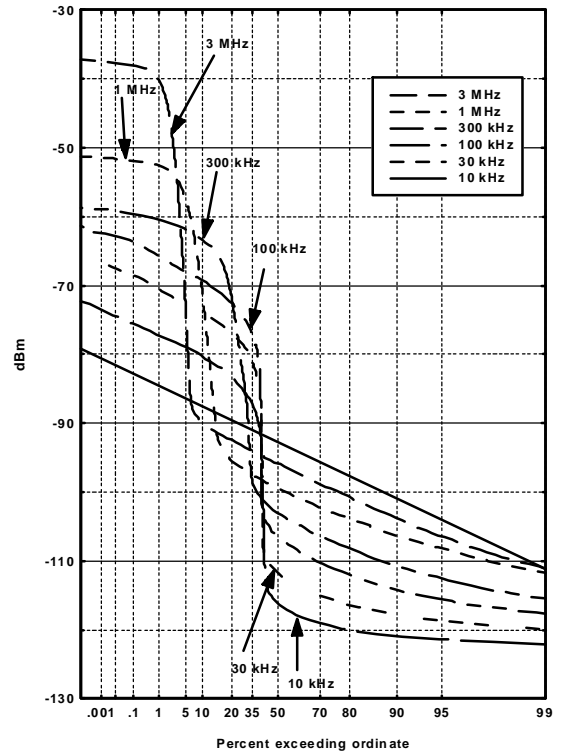


Figure 8.29. Device B APDs, 128 kb/s.

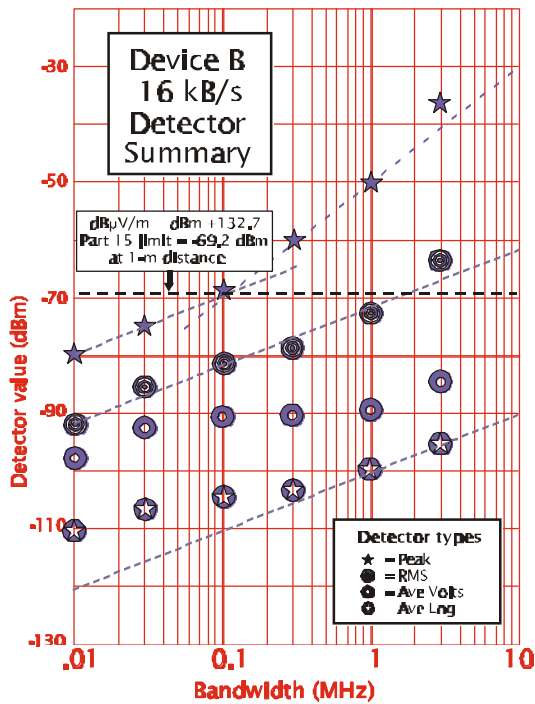


Figure 8.30. Device B detector summary, 16kb/s.

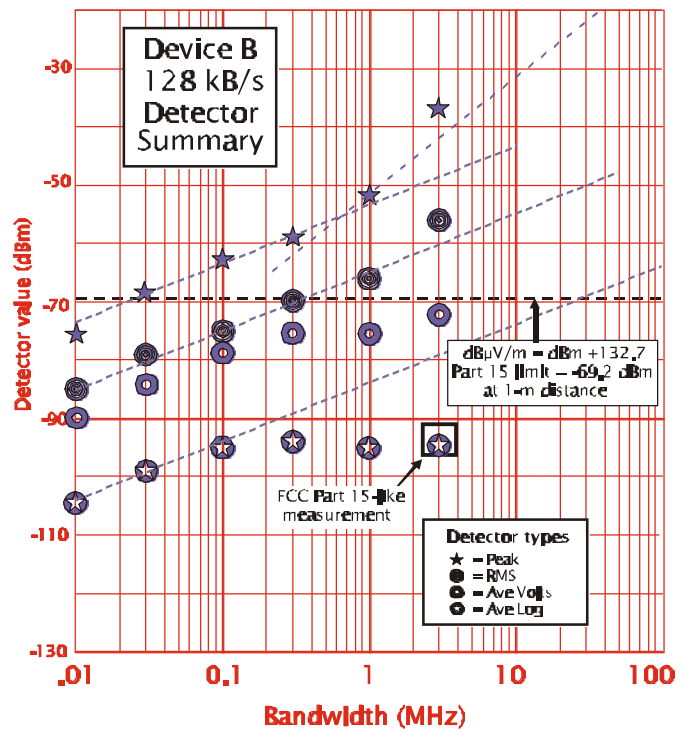


Figure 8.31. Device B detector summary, 128 kb/s.

8.3.3 Summary of Device C Measurements

Device description. Device C transmits an ungated 2-MHz PRR pulse train over the 1-5 GHz range. Device C uses a “relative” dithering technique. This dithering technique uses only a small amount of pulse delay (in this case, 1.25% delay out of 500 ns average pulse spacing), but timing is referred to the preceding pulse instead of being referred to a fixed time base. Figures 8.32 to 8.35 show how a continually larger timing variation builds up over elapsed time, until the 1.25% delay (494-500 ns) for individual pulse-to-pulse spacing covers the entire pulse-to-pulse interval.

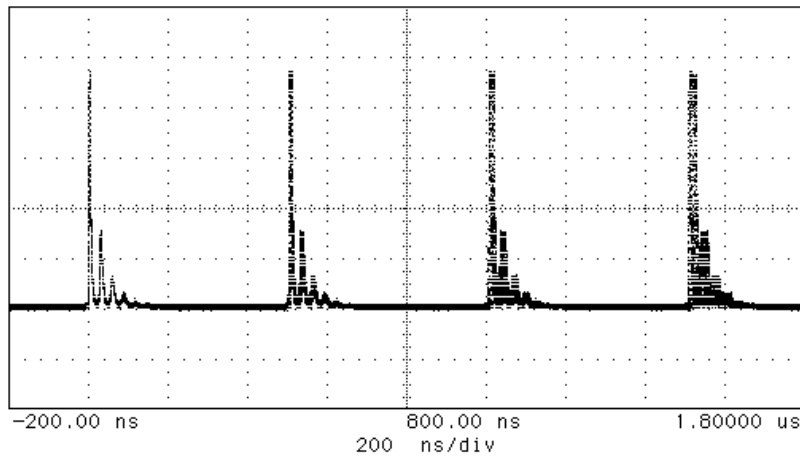


Figure 8.32. Device C dither at starting point.

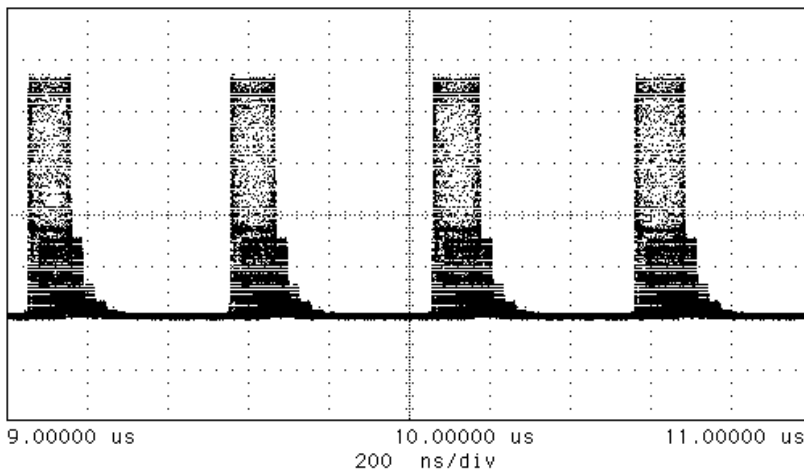


Figure 8.33. Device C dither 20 pulses after zero point.

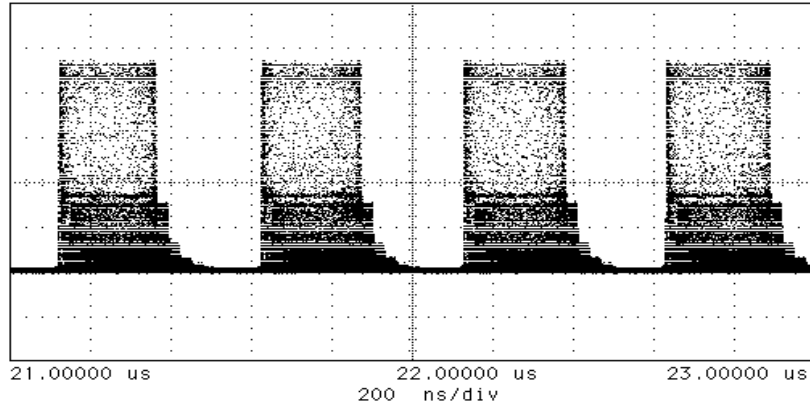


Figure 8.34. Device C dither 44 pulses after zero point

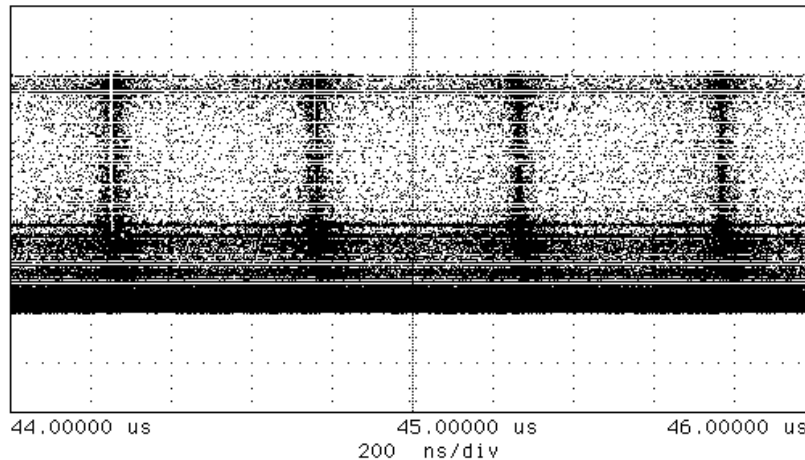


Figure 8.35. Device C dither 90 pulses after zero point

Full-bandwidth pulse shape. Figure 8.36 shows a complex pulse with extended ringing.

FFT emission spectra. Figure 8.37 shows a well-defined emission about 600 MHz wide and centered at about 1800 MHz. The calculated peak radiated field strength is approximately 86 dB μ V/m in a 20-MHz bandwidth..

Narrowband peak emission spectra. Figure 8.38 shows emission spectra with a peak about 700 MHz wide, centered at about 1800 MHz, though the details appear somewhat different from the FFT spectrum. The 20-MHz bandwidth measurements show a measured peak field strength of 87 dB μ V/m, closely matching the FFT spectrum.

Spectrum fine structure. Figure 8.39 shows a subtle set of fine structures related to the 2-MHz average PRR. The relative dithering technique appears to be effective in eliminating 2-MHz discrete spectral lines that extend above the surrounding spectrum. The signals at all frequencies

appear to have about the same maximum power, with a mix of amplitudes that are distributed across a range between the maximum and as much as 30 dB below the maximum. However, there is a pattern of higher-than-average-power frequencies repeated every 2 MHz, where the average signal power is maximized by spending less time at the lower amplitudes. These higher-than-average-power frequencies were designated “on-spectral-lines” frequencies, and intermediate frequencies with less average power were designated “between-spectral-lines” frequencies.

Bandwidth progression stairsteps. Figure 8.40 shows a bandwidth progression measurement made at an “on-spectral-lines” frequency. This measurement shows impulsive behavior at 3-MHz bandwidth, CW-like results for bandwidths between 100 kHz and 1 MHz, and noise-like behavior for narrower bandwidths.

Gating, PRR, and modulation. Figure 8-41 shows a measurement of the Device C pulse train, which exhibits no obvious pulse position modulation. Figures 8-42 and 8-43 show the modulated IF waveforms at 1-MHz and 100-kHz bandwidths. Surprisingly, the 100-kHz waveform contains much more amplitude modulation than the 1-MHz waveform.

APDs. APDs were measured at between-spectral-lines and on-spectral-lines frequencies – Figures 8-44 and 8-45, respectively. Measurements for the between-spectral-lines case were also made using 10-MHz and 20-MHz bandwidths.

Detector summaries. The two APDs and the corresponding detector summaries (Figures 8-46 and 8-47) show some interesting results. The two dashed lines on each detector summary are drawn as best-fit trend lines for the RMS detectors for the on-spectral-lines and between-spectral-lines measurements, showing about 2.5-dB difference between the two cases. The 3-MHz on-spectral-lines RMS value drops to the between-spectral-lines trend line, showing that the effect of the relatively narrow bandwidth concentration of on-spectral-lines energy disappears when the measurement bandwidth is widened beyond the 2-MHz fine structure.

The between-spectral-lines detector summary shows a large divergence between different detector values at 100-kHz bandwidth, including a 15-dB difference between average logarithm and RMS and a 27-dB difference between average logarithm and peak. The minimum difference between detector values occurs at 1-MHz bandwidth, where there is only a 6-dB difference between average logarithm and peak values. These results are particularly interesting (and somewhat counterintuitive) because they illustrate a UWB modulation technique that produces impulse-like results (i.e., wide divergence between detector values) at lower bandwidths and CW-like results at higher bandwidths. The proposed FCC Part 15 limits, however, assume that a UWB signal will appear more CW-like at lower bandwidths (average limit specified in 1-MHz bandwidth), and more impulsive at higher bandwidths (peak limit specified in $B = 50$ MHz).

FCC Part 15 measurements. Part 15 measurements were made at the “on-line” frequency using a 300-Hz video filter, which produced a signal with about 0.5 dB peak-to-peak ripple and a peak amplitude of -74 dBm. This compares with a computed average logarithm of -74.2 dBm.

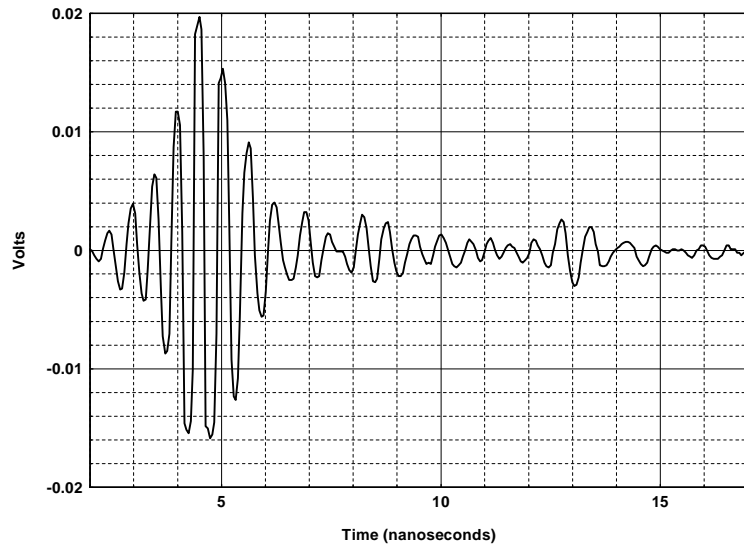


Figure 8.36. Device C full bandwidth pulse shape.

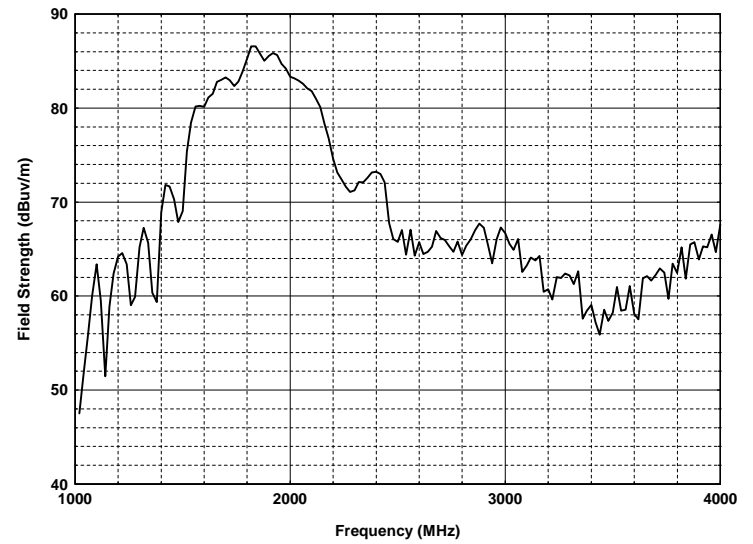


Figure 8.37. Device C, radiated peak field strength at 1 m, $f = 20$ MHz.

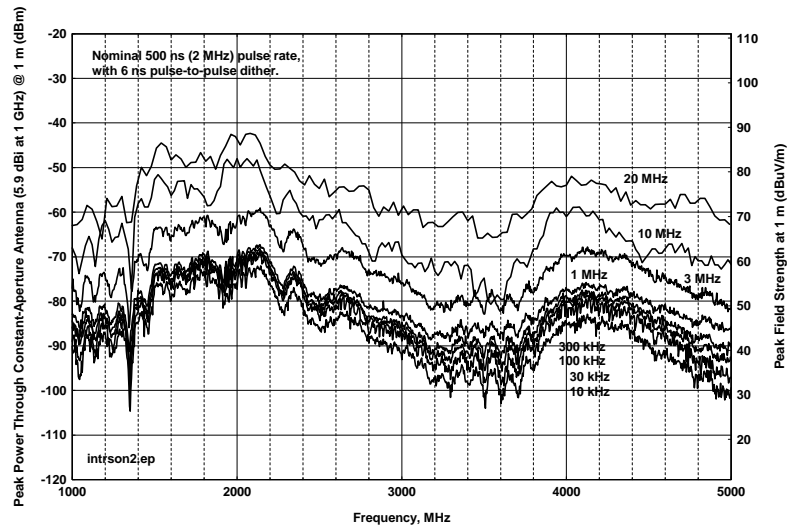


Figure 8.38. Device C spectra in multiple bandwidths.

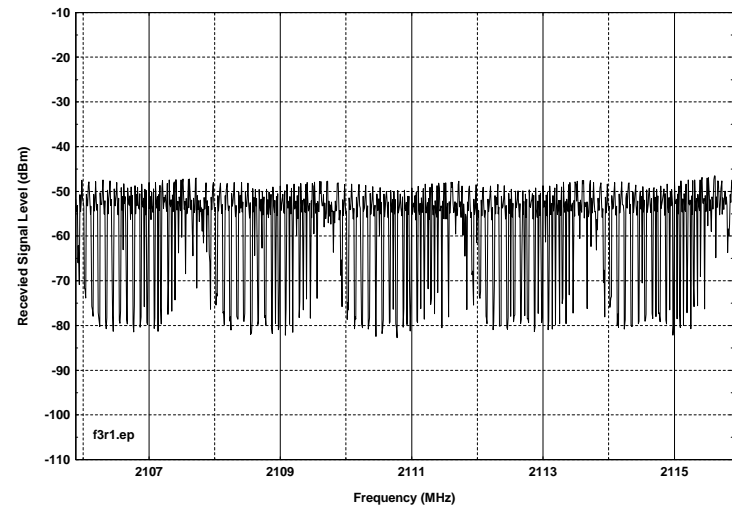


Figure 8.39. Device C, peak-detected to show spectral line patterns in noise.

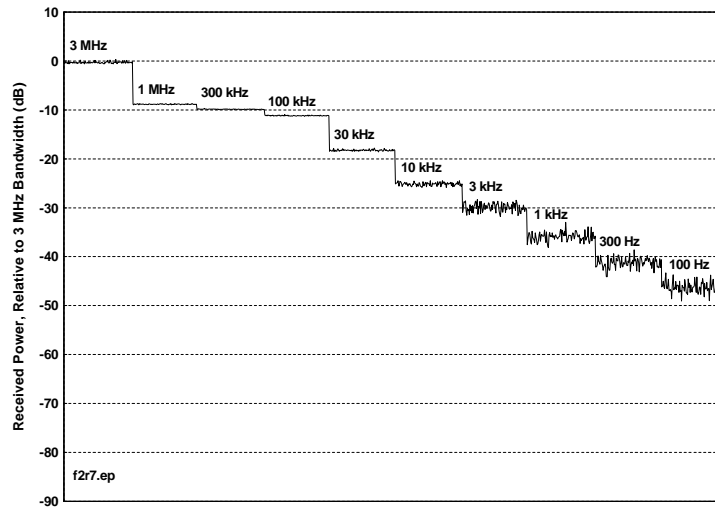


Figure 8.40. Device C, peak bandwidth progression staircase.

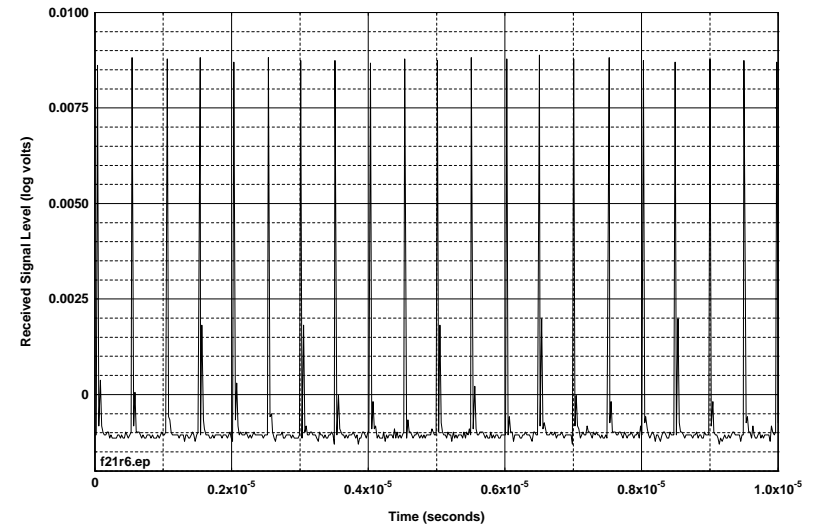


Figure 8.41. Device C, pulse train waveform for 10 microseconds, external detector.

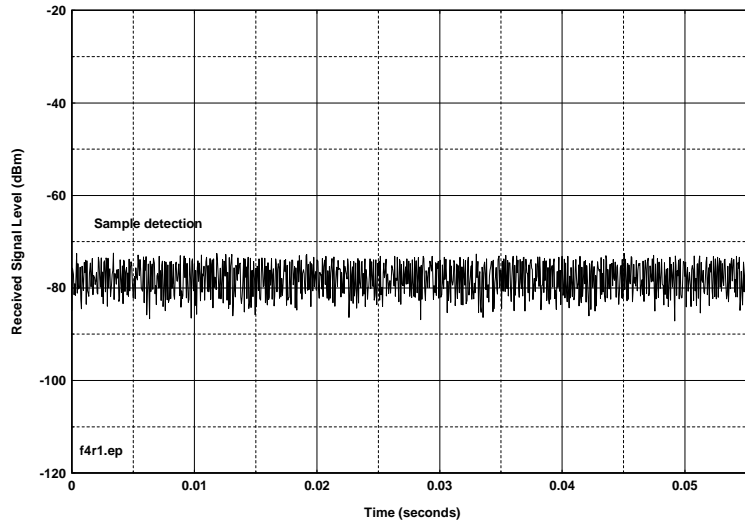


Figure 8-42. Device C, time waveform in 55 ms, 3-MHz IF bandwidth.

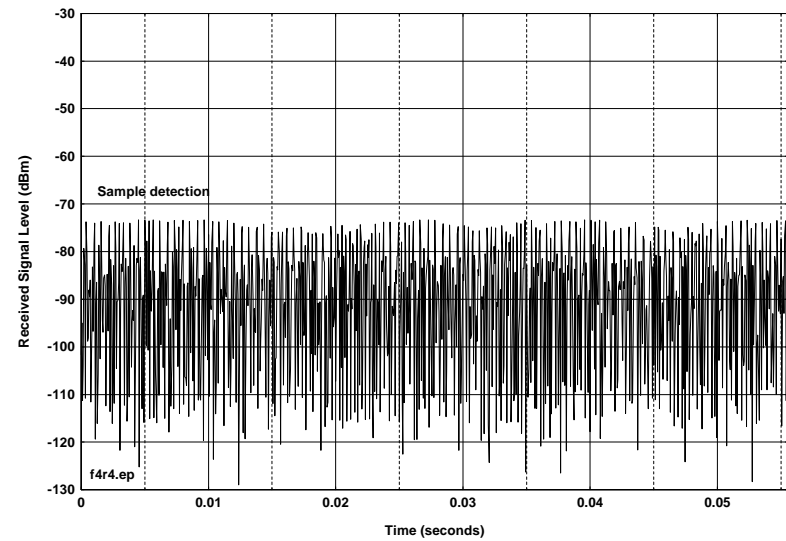


Figure 8.43. Device C, time waveform in 55 ms, 100-kHz IF bandwidth.

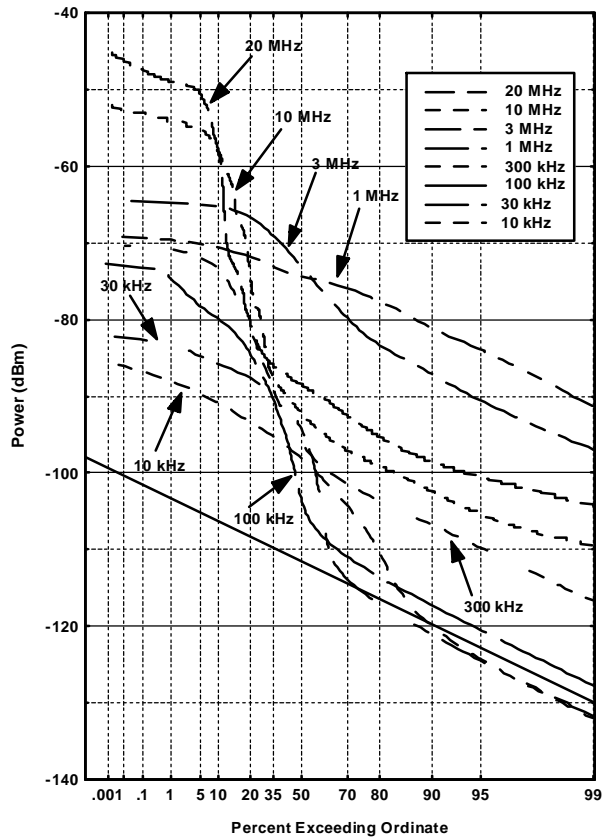


Figure 8.44. Device C APDs, between spectral lines.

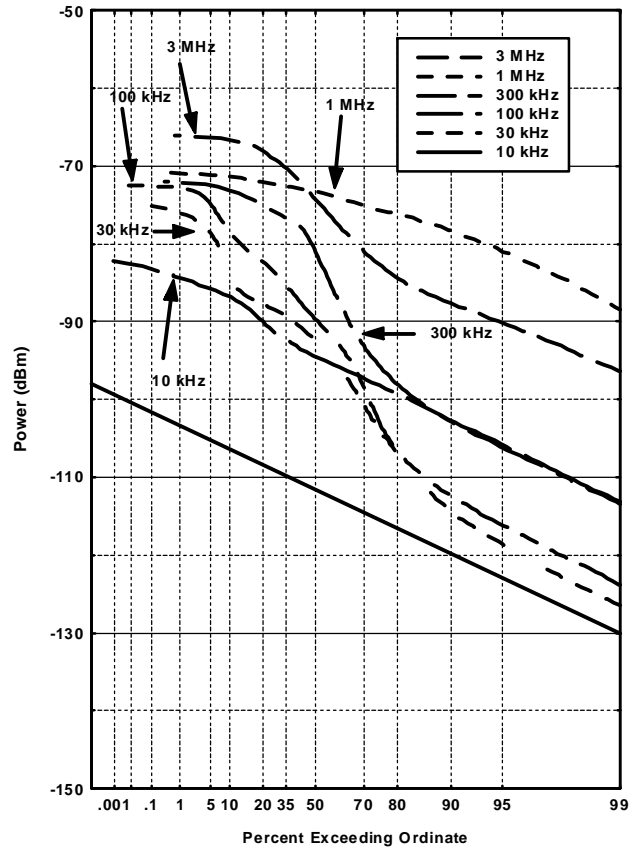


Figure 8.45. Device C APDs, on spectral lines.

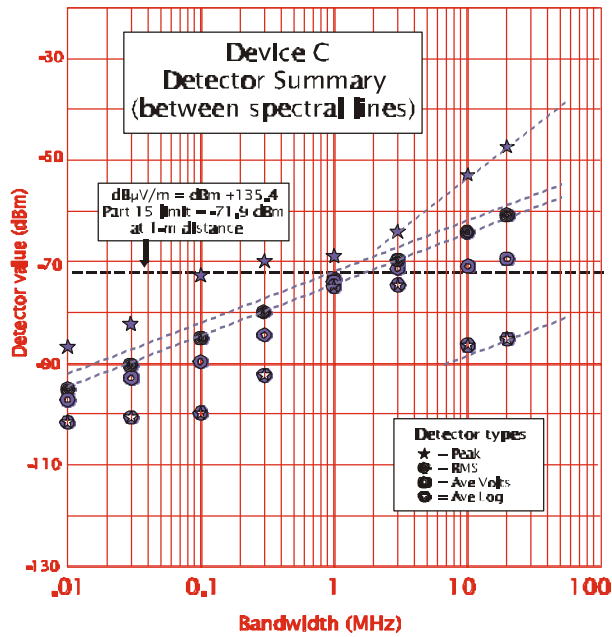


Figure 8.46. Device C, detector summary (between spectral lines).

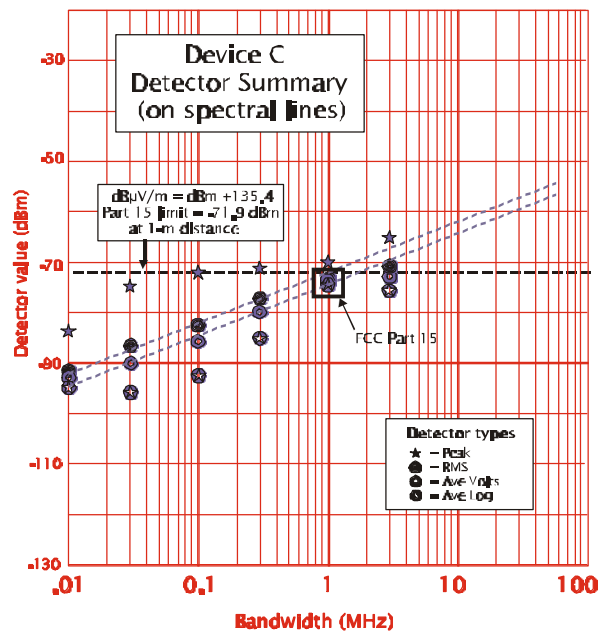


Figure 8.47. Device C, detector summary (on spectral lines)

8.3.4 Summary of Device D Measurements

Device Description: Device D operates with basic PRRs of 1 MHz, 5 MHz, and 10 MHz, with gating duty cycles available between 25% and 100% (continuously on). A fixed 25% dither is applied, using an absolute time base in all modes. The device was measured in four modes: 1-MHz PRR, 25% gated duty cycle; 1-MHz PRR, 100% gated duty cycle; 10-MHz PRR, 25% gated duty cycle; and 10-MHz PRR, 100% gated duty cycle. The gating cycle for both PRRs utilized a 2-ms “on” period and a 6-ms “off” period. This data transmission device was measured without transmitting any actual data.

Full-bandwidth pulse shape and FFT spectrum. The Device D radiated full-bandwidth pulse shape (Figure 8.48) was used to compute an FFT peak spectrum over the 1-4 GHz range (Figure 8.49).

Narrowband peak emission spectra. Figures 8.50-8.53 contain spectrum measured for each of four Device D operating modes. These spectra compared closely in shape and amplitude with the FFT spectrum. Figure 8.53 included measurements made in a 20-MHz bandwidth, which show close agreement (within 1-2 dB) with the FFT values computed in a 20-MHz bandwidth.

Bandwidth progression staircase. The stair-step bandwidth progression graphs (Figures 8.54-8.57) were measured at a frequency near 1560 MHz and show substantial differences between the 1-MHz PRR and the 10-MHz PRR modes. These differences are likely caused by the higher power and greater frequency separation of the discrete spectral lines in the 10-MHz PRR modes.

Spectrum fine structure. Details of the spectrum fine structure showed strong lines with 1-kHz spacing in the 1-MHz PRR mode (Figure 8.58) and 10-kHz spacing in the 10-MHz PRR mode (Figure 8.59). It is not known whether these lines would be present with transmission of actual data. Figure 8-60 shows pulse-position modulation, measured in a 10-MHz bandwidth.

APDs. The APDs are shown in Figures 8.62 to 8.65. The non-gated modes (100% gating) appear like Gaussian noise for bandwidths less than the PRR and appear impulse-like for bandwidths larger than the PRR. The gated modes show clear break-points at the 25% point, with measurement system noise present for the remaining 75% of the duration.

Detector summary. The detector summaries (Figures 8.66 to 8.69) show that the ungated modes appeared similar to Gaussian noise for bandwidths less than the PRR. For all narrower bandwidths, peak values were about 10-dB greater than the RMS, and the average voltage and average logarithm were tightly clustered within a few dB less than the RMS. All of the detector functions followed a $10 \log_{10} B$ trend line. The corresponding trend lines were 8-10 dB higher for the 10-MHz PRR than for the 1-MHz PRR mode. Only when the bandwidth was greater than the PRR, did the detector values at a bandwidth begin to diverge. The peak values then followed a $20 \log_{10} B$ trend. The average logarithm and average voltage decreased substantially at larger bandwidths, when pulses did not overlap and system noise was momentarily the only signal.

The gated modes provided peak values identical to the corresponding ungated (i.e.,100%) modes. The gated RMS values were approximately 6 dB lower than those of the corresponding ungated modes, as expected when the total number of impulses was decreased by 75%. The gated mode average logarithm dropped to within a few dB of system noise (present 75% of the time), with the 10-MHz PRR average logarithm being 1-2 dB higher than the 1-MHz logarithm.

FCC Part 15 Measurements. Part 15 measurements for the ungated 1-MHz PRR and 10-MHz PRR modes matched the average logarithms at -84 dBm and -74 dBm, respectively. Part 15 measurements for the gated modes were -100 dBm and -97 dBm for the 1-MHz PRR mode and 10-MHz PRR mode (Figure 8.61), respectively. The 1-2 dB discrepancy between Part 15 and average logarithm for gated modes was caused by insufficient video filtering of the 8 ms gating cycle, which allowed 2-3 dB of ripple on the video filter output.

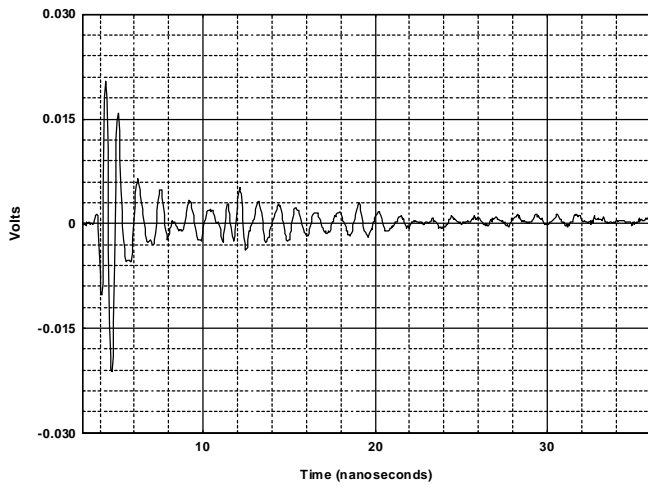


Figure 8.48. Device D radiated full-bandwidth pulse shape

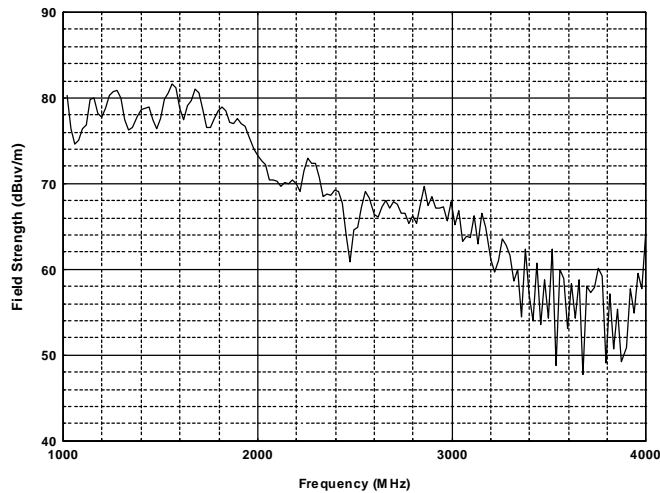


Figure 8.49. Device D, radiated peak field strength at 1 m,) f = 20 MHz.

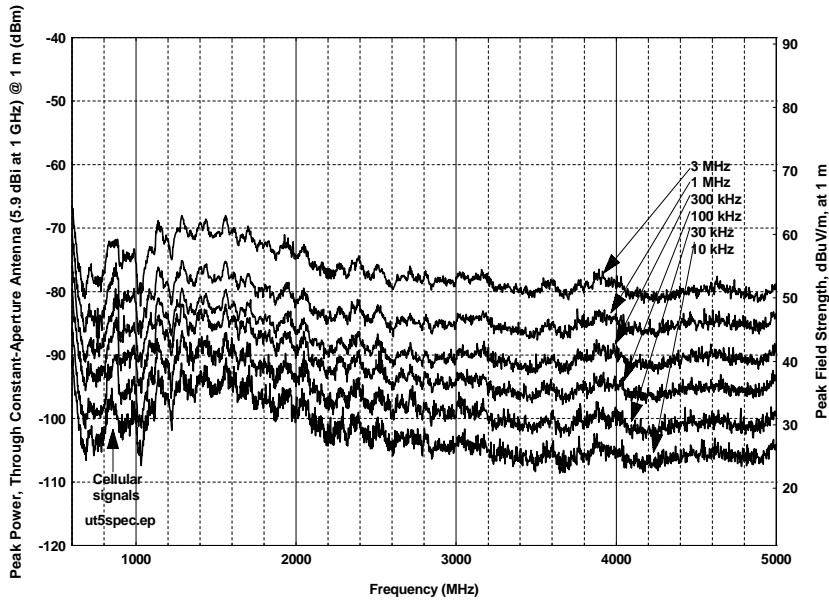


Figure 8.50. Device D spectra, 1-MHz PRR, 25% gating.

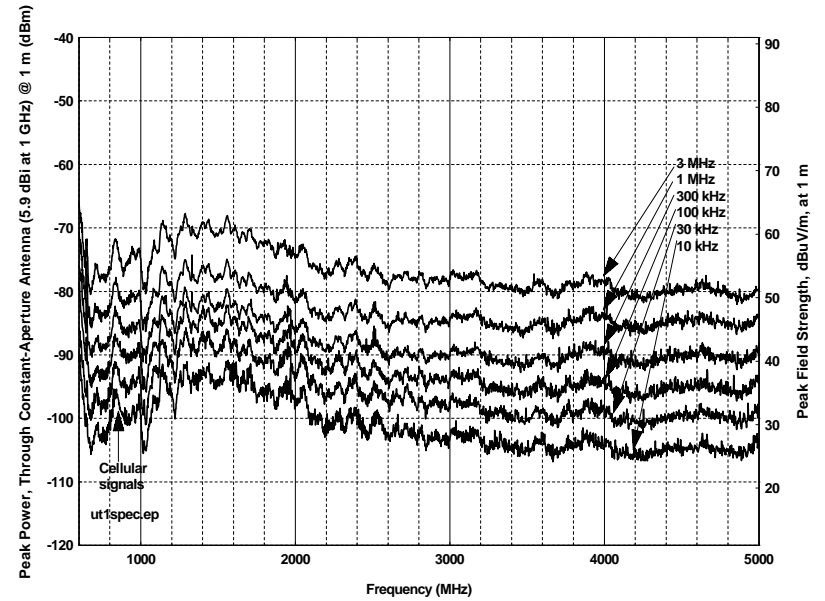


Figure 8.51. Device D spectra, 1-MHz PRR, 100% gating.

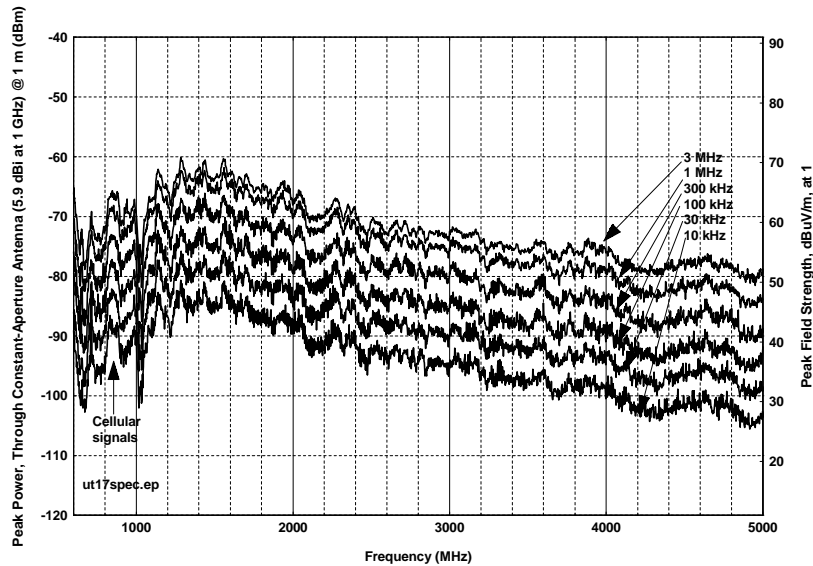


Figure 8.52. Device D spectra, 10-MHz PRR, 25% gating.

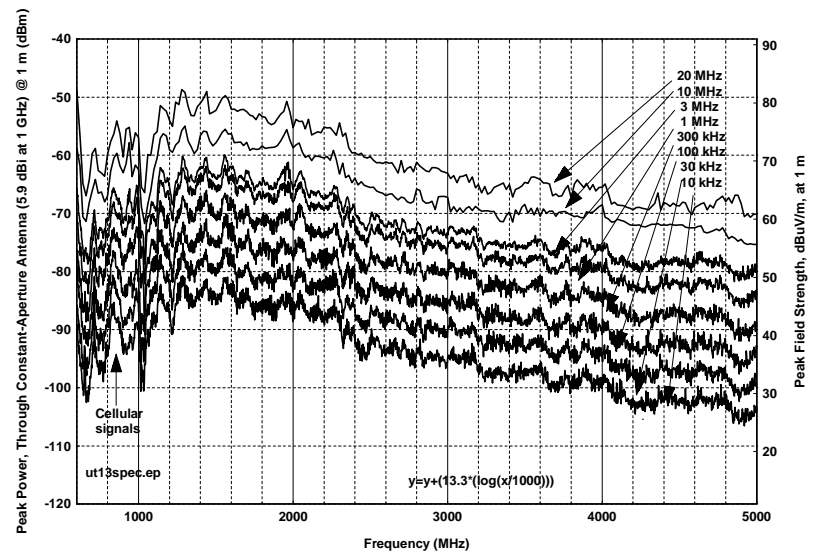


Figure 8.53. Device D spectra, 10-MHz PRR, 100% gating.

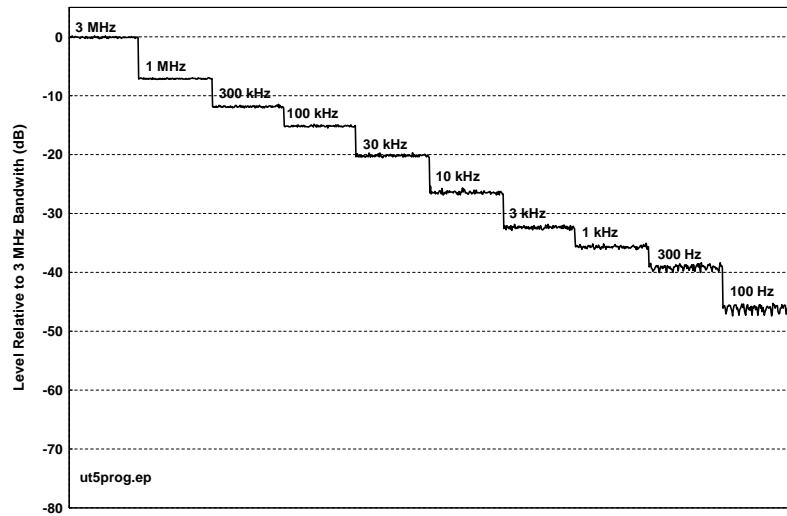


Figure 8.54. Device D bandwidth progression stairstep, 1-MHz PRR, 25% gating.

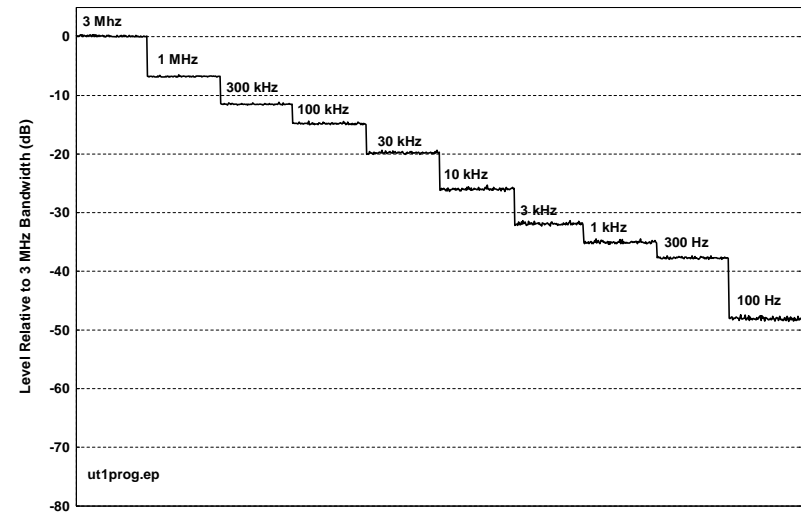


Figure 8.55. Device D bandwidth progression stairstep, 1-MHz PRR, 100% gating.

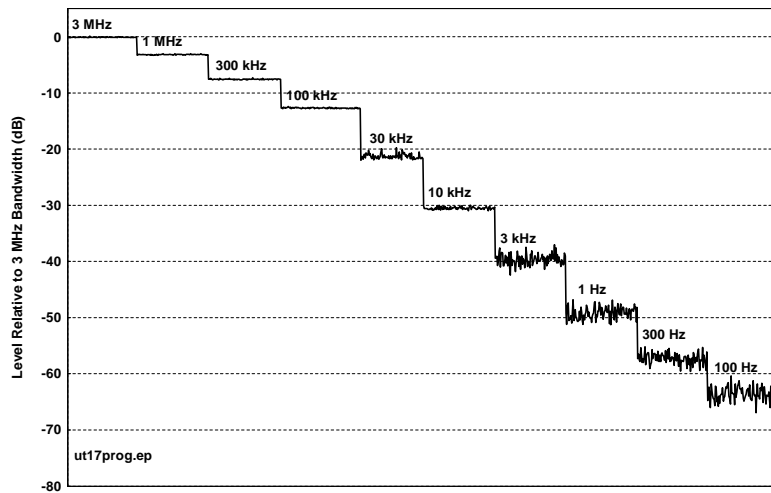


Figure 8.56. Device D bandwidth progression stairstep, 10-MHz PRR, 25% gating.

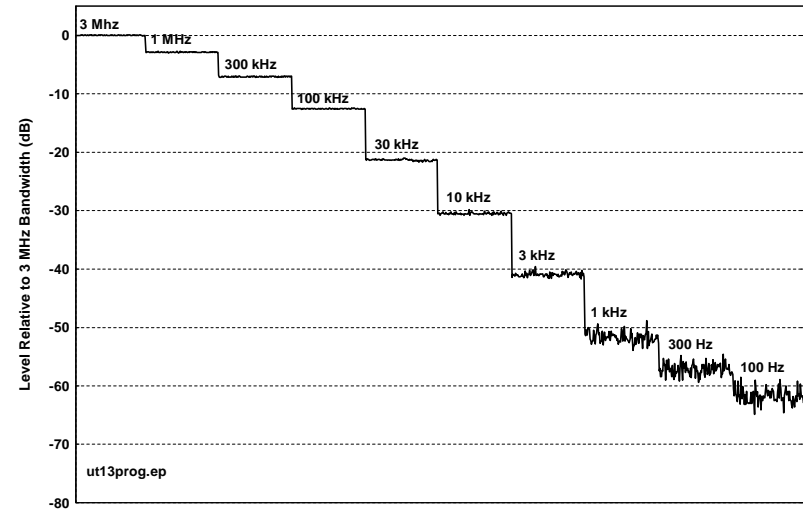


Figure 8.57. Device D bandwidth progression stairstep, 10-MHz PRR, 100% gating.

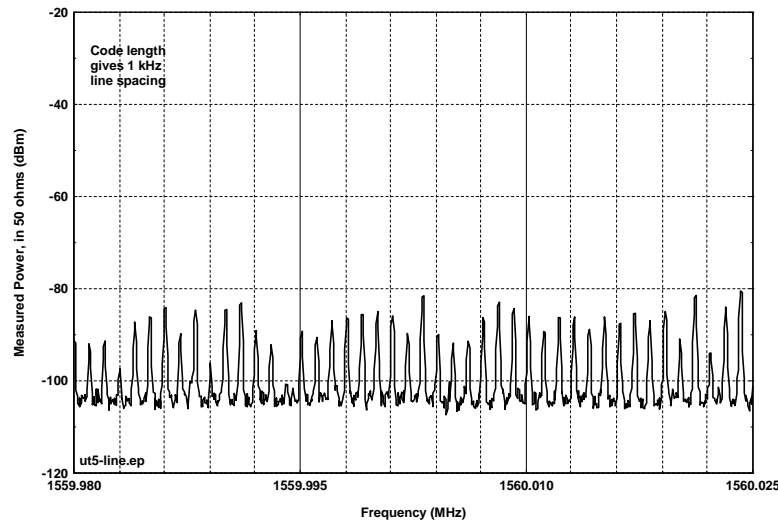


Figure 8.58. Device D 1-kHz emission lines, 1-MHz PRR, 25% gating.

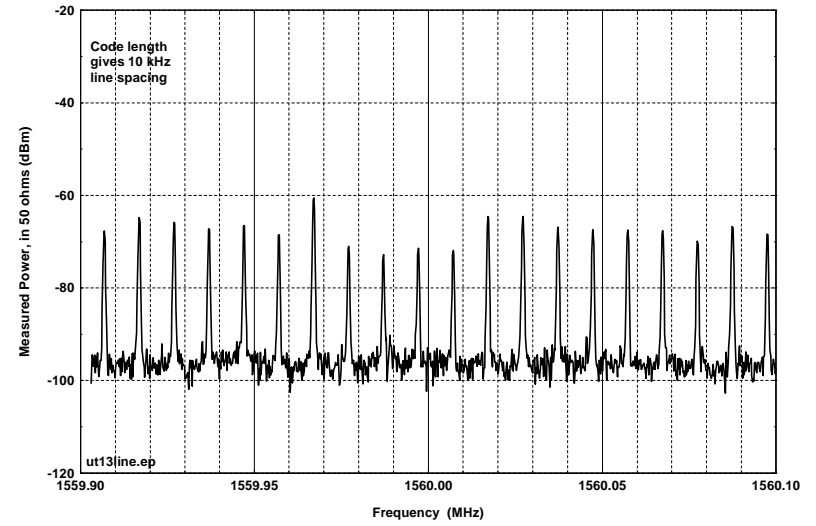


Figure 8.59. Device D 10-kHz emission lines, 10-MHz PRR, 100% gating.

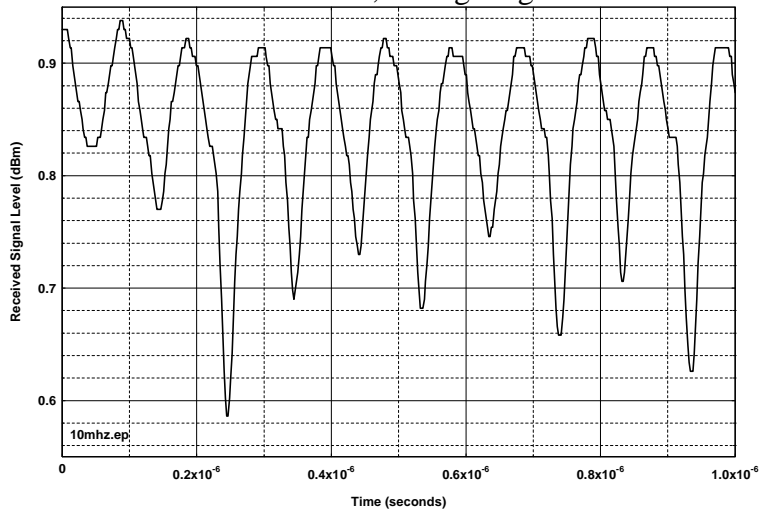


Figure 8.60. Device D waveforms, 10-MHz IF, 10-MHz PRR, 100% gating, 25% dither, showing pulse position modulation.

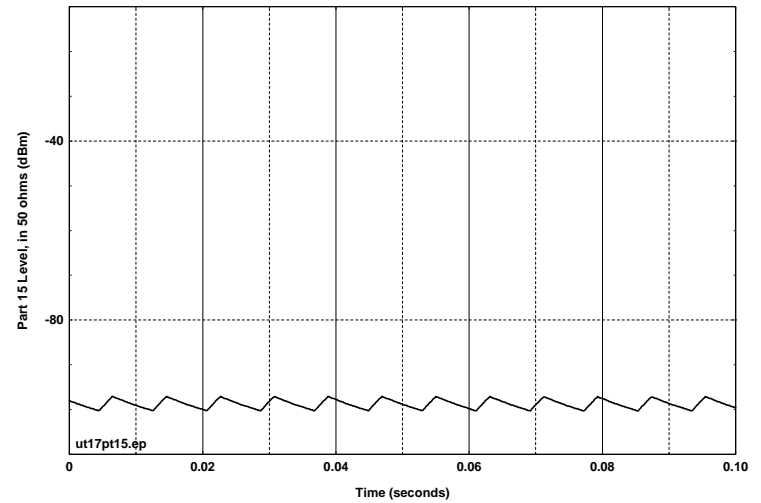


Figure 8.61. Device D, 10-MHz PRR, 25% gating, Part 15 measurement showing ripple in 10-Hz video BW.

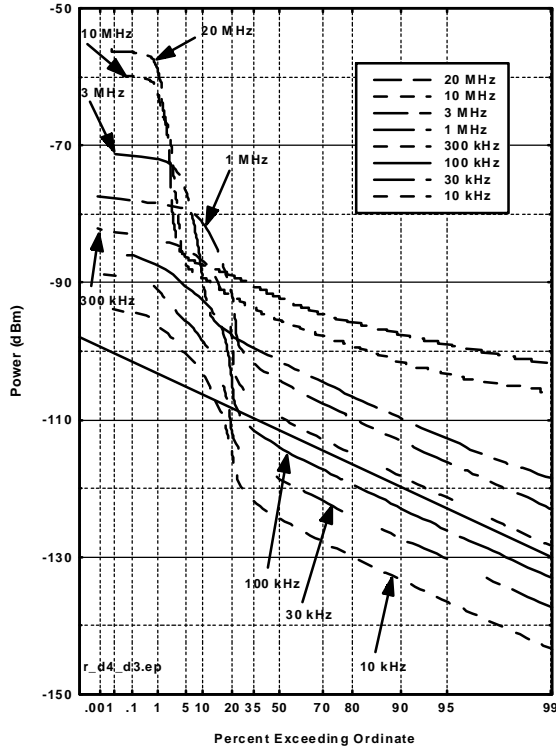


Figure 8-62. Device D APDs, 1-MHz PRR, 25% gating.

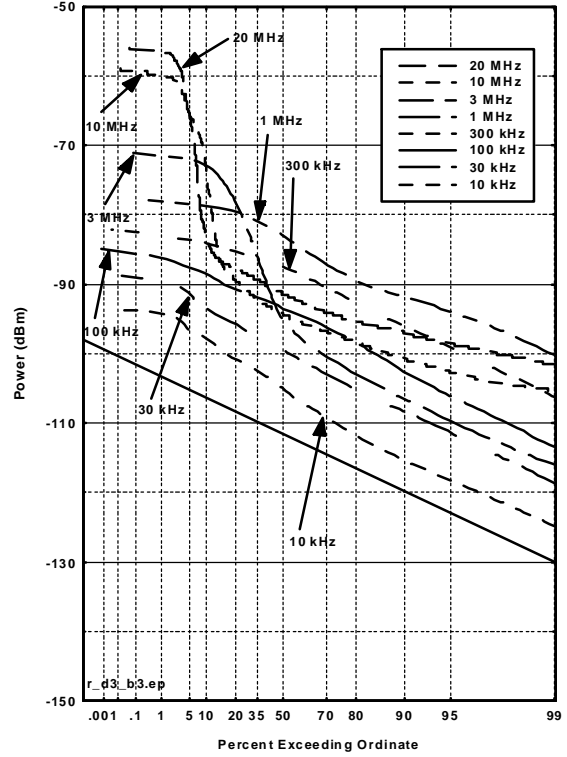


Figure 8.63. Device D APDs, 1-MHz PRR, 100% gating.

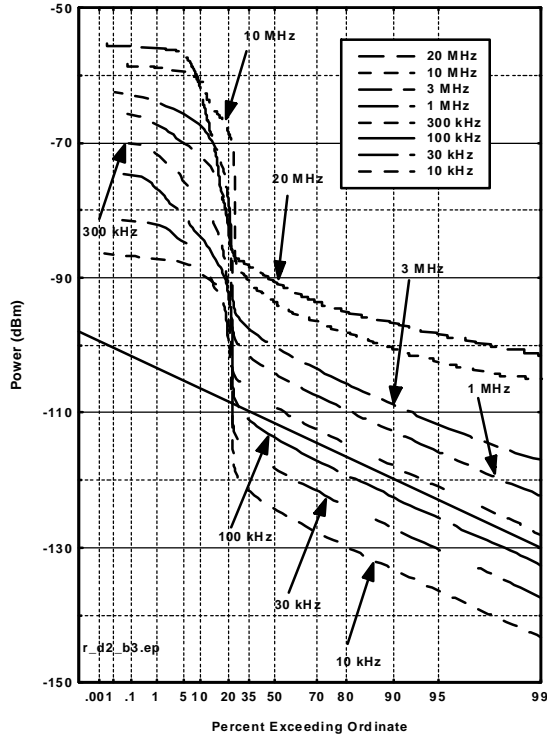


Figure 8.64. Device D APDs, 10-MHz PRR, 25% gating.

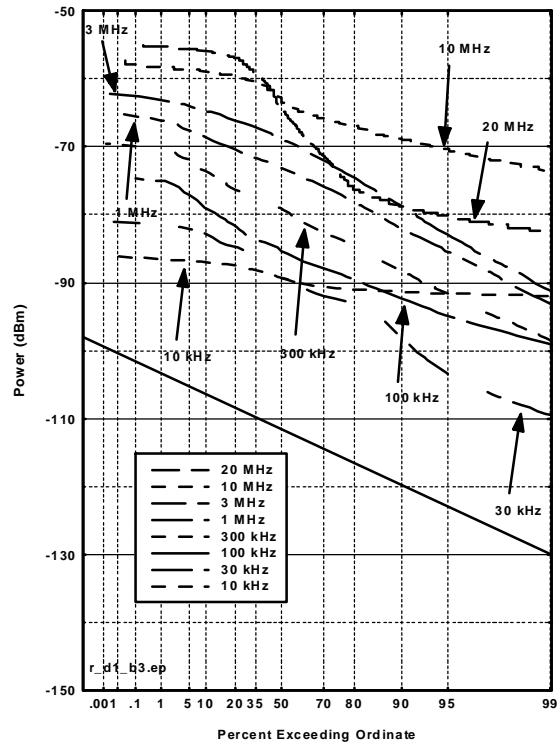


Figure 8.65. Device D APDs, 10-MHz PRR, 100% gating.

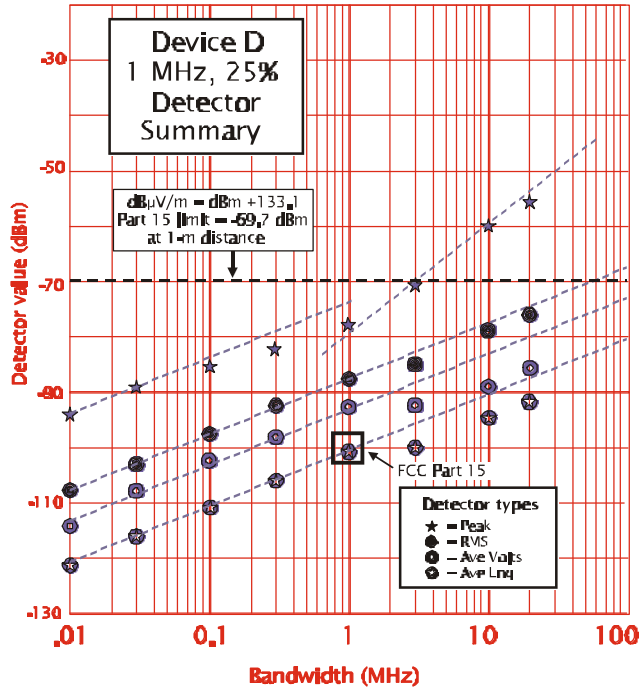


Figure 8.66. Device D detector summary, 1-MHz PRR, 25% gating.

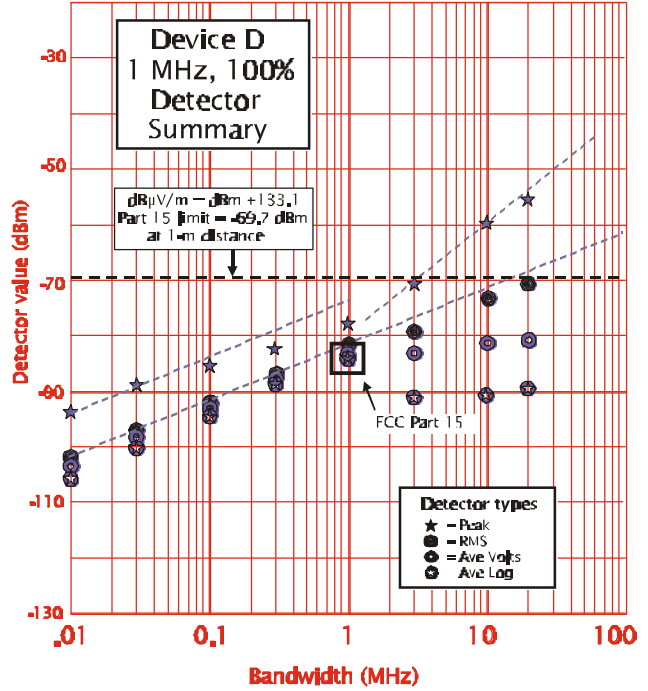


Figure 8.67. Device D detector summary, 1-MHz PRR, 100% gating.

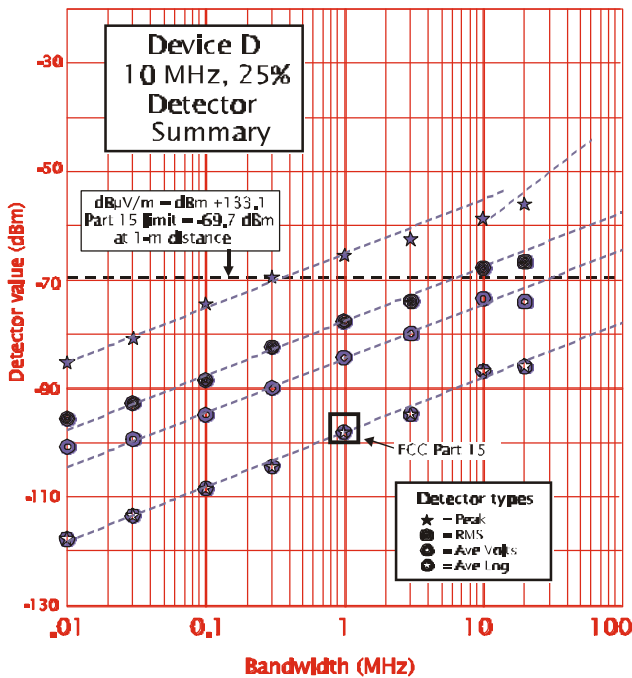


Figure 8.68. Device D detector summary, 10-MHz PRR, 25% gating.

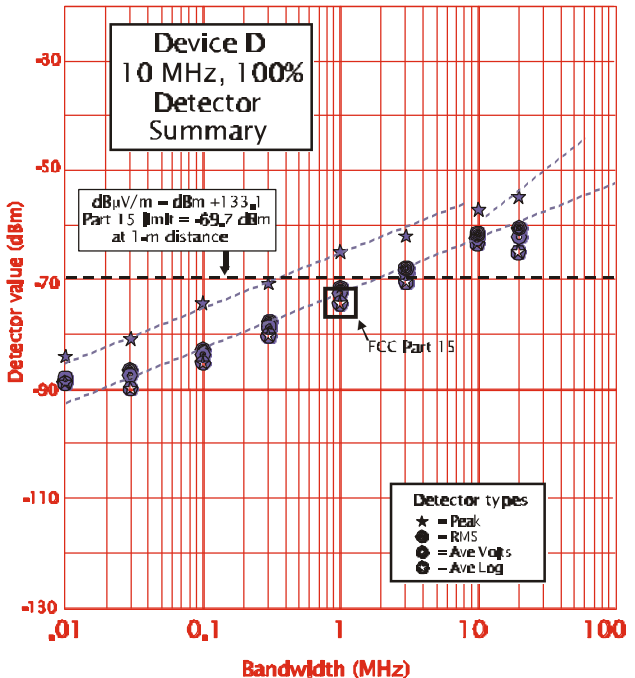


Figure 8.69. Device D detector summary, 10-MHz PRR, 100% gating.

8.3.5 Summary of Device E Measurements

Device description: Device E is designed to radiate mainly towards the ground. Interchangeable RF heads permitted operation at nominal frequencies of 300 MHz, 900 MHz, and 1500 MHz.. Device E is capable of operating with multiple PRRs.

Full-bandwidth pulse shapes. Full-bandwidth pulse shape measurements were made with all three RF heads (Figures 8.69, 8.71, and 8.73), with the Device E antennas aimed directly at the measurement antenna 1 m away. These pulse shapes are very simple, with no additional lobes or extended ringing.

FFT emission spectra. FFT spectra were computed from each of the measured pulse shapes (Figures 8.70, 8.72, and 8.74, respectively).

Narrowband peak emission spectra. Spectrum analyzer measurements were made only with the 1500-MHz head, with Device E resting on a concrete floor, aiming downwards, with the measurement antenna 1 meter away from the edge of Device E and slightly above the floor. The spectrum analyzer measurements signal amplitudes cannot be compared with the FFT spectra because of different measurement conditions.

Bandwidth progression staircase. Figure 8.76 shows the Device E emission spectrum, using the 1500- MHz RF head..

Gating, PRR, and modulation. The mode that was measured included a PRR near 85 kHz and a gating duty cycle of approximately 25 ms on, 6 ms off (Figures 8-78 and 8-79).A distinguishing feature of the Device E spectrum analyzer measurements was relatively low received power, which prevented Part 15 measurements from being made, and which also made it difficult to see some details of the modulation.

APDs. Figure 8.80 show APD measurements for the Device E 1500-MHz RF head.

Detector summary. Figure 8.81 shows a detector summary for Device E. Detector values for bandwidths less than 1 MHz seem to be mostly measurement system noise.

FCC Part 15 measurements. The signal from Device E was apparently below measurement system noise and Part 15 measurements could not be performed.

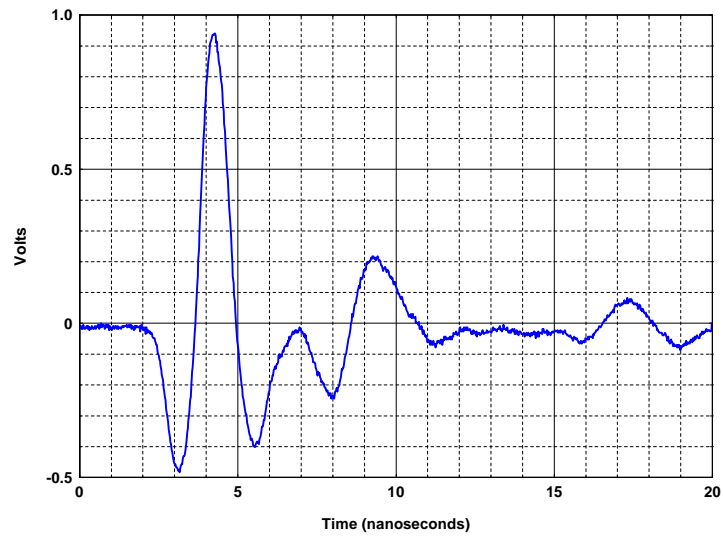


Figure 8.70. Device E full bandwidth pulse shape, 300-MHz RF head, main beam.

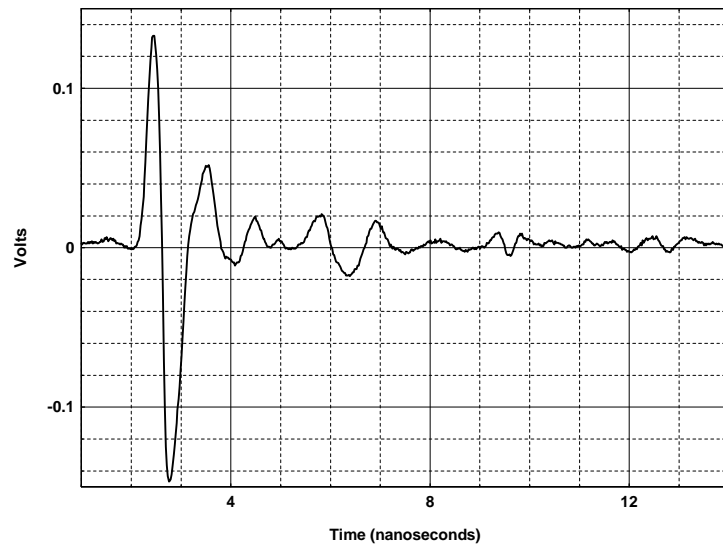


Figure 8.72. Device E full bandwidth pulse shape, 900-MHz RF head, main beam.

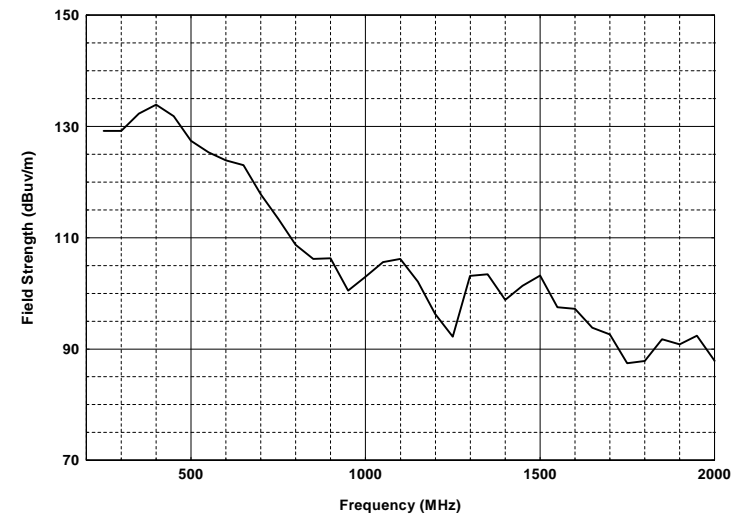


Figure 8.71. Device E, (300-MHz head), peak field strength at 1 m, main beam,) $f = 50$ MHz.

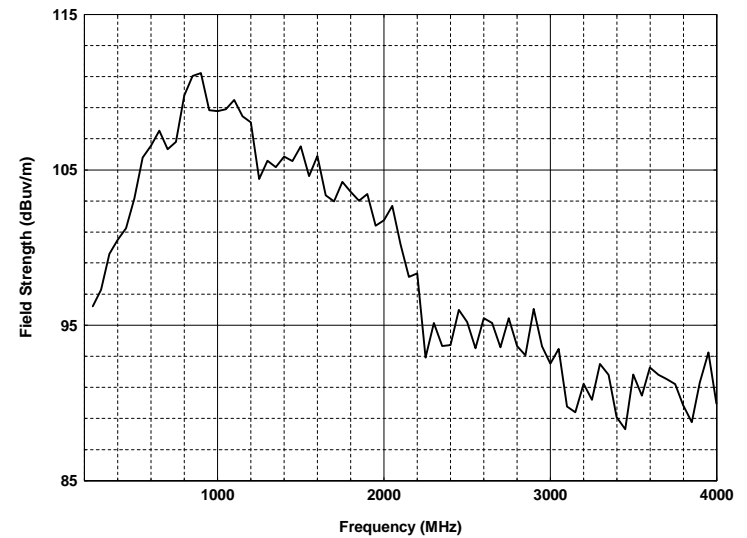


Figure 8.73. Device E (900-MHz head) peak field strength at 1 m, main beam,) $f = 50$ MHz.

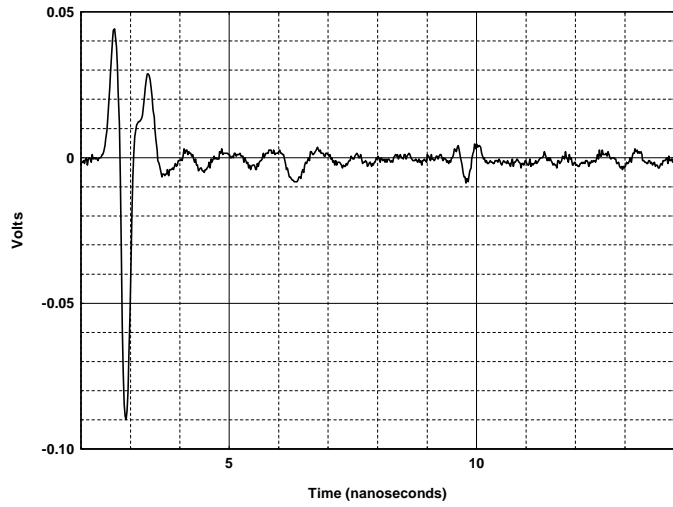


Figure 8.74. Device E full bandwidth pulse shape, 1500-MHz RF head, main beam.

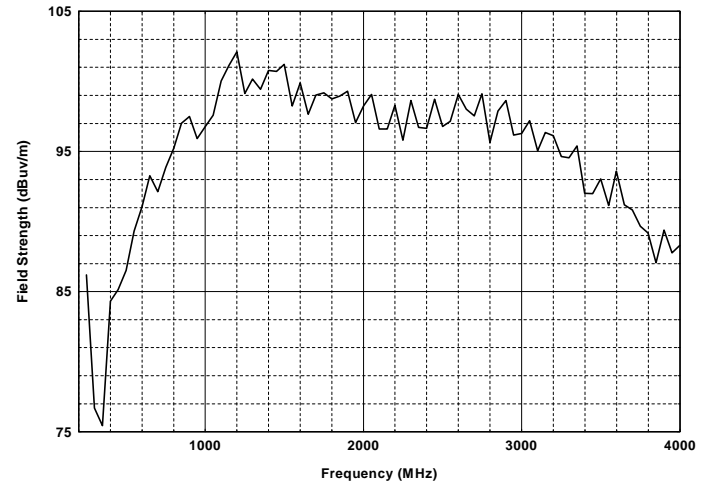


Figure 8.75. Device E (1500-MHz head) peak field strength at 1 m, main beam,) f = 50 MHz.

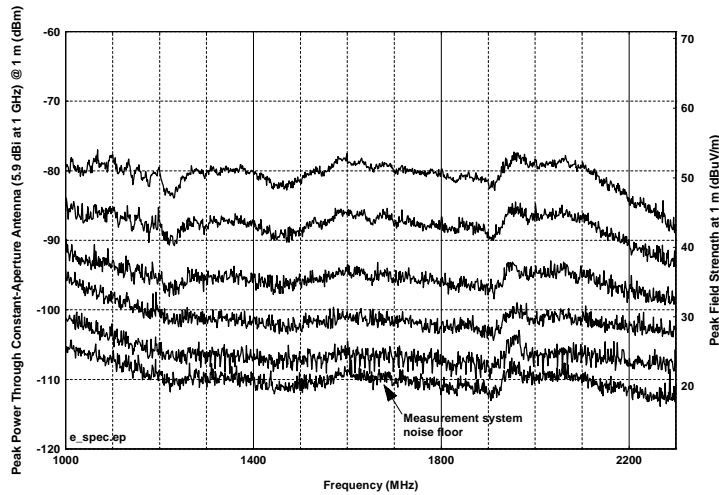


Figure 8.76. Device E 1500-MHz RF head, spectra as a function of measurement bandwidth.

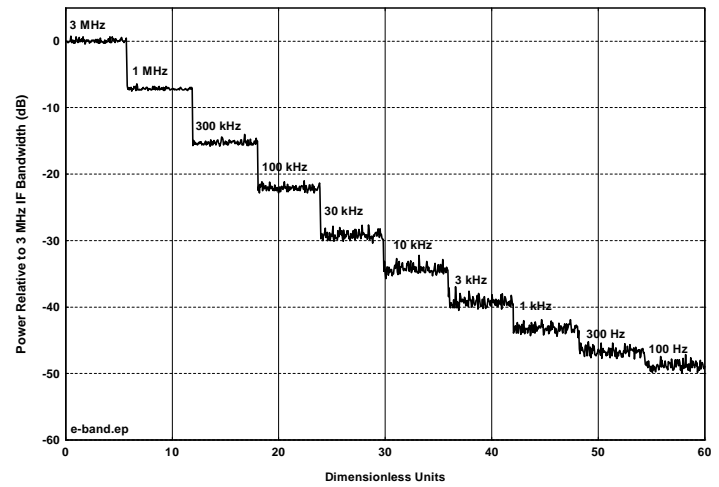


Figure 8.77. Device E 1500-MHz RF head, peak bandwidth progression staircase.

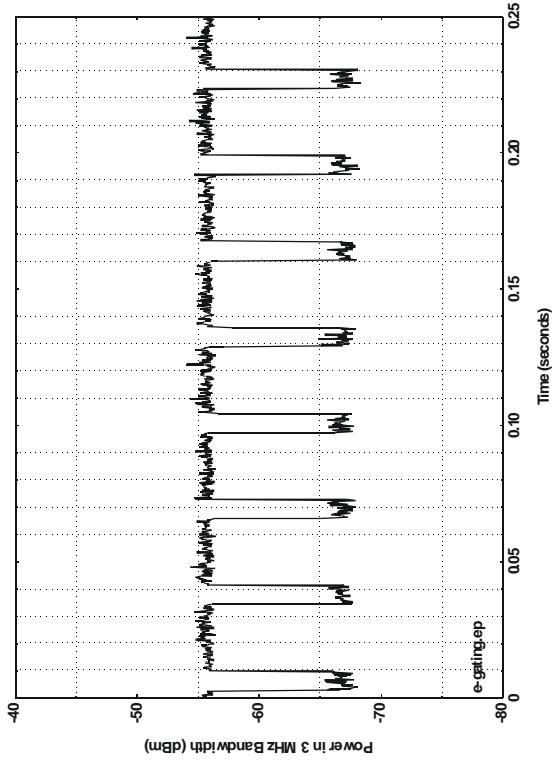


Figure 8.78. Device E pulse train.

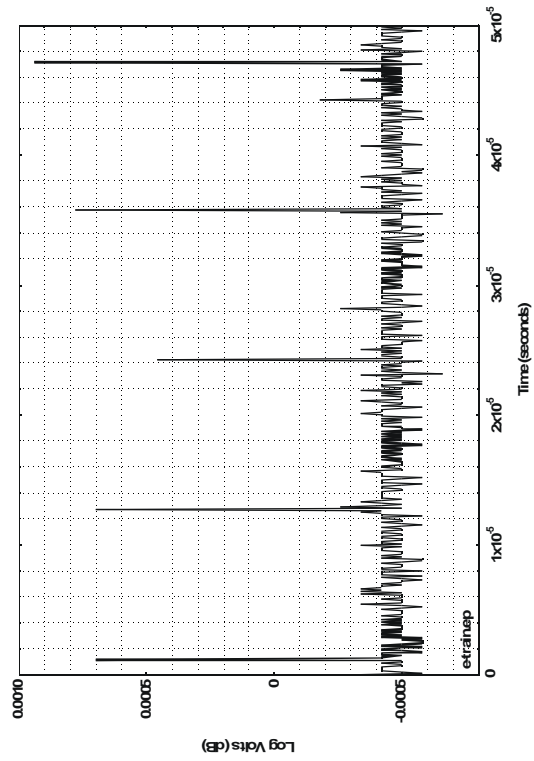


Figure 8.79. Device E gating waveform.

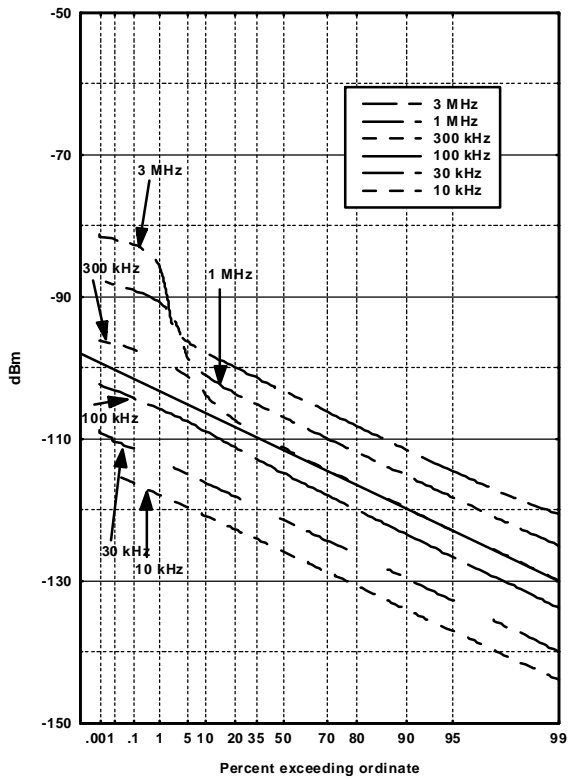


Figure 8.80. Device E APDs.

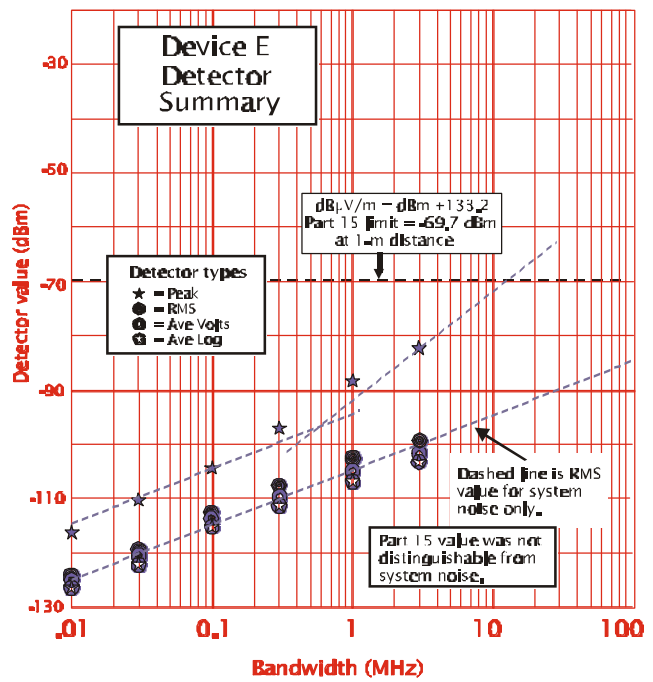


Figure 8.81. Device E, detector summary.

8.3.6 Summary of Electric Drill Measurements

An electric drill is included in the category of Part 15 Incidental Radiators, since it radiates radio frequency energy, although its function does not require the generation of radio frequency signals. The electric drill controls included only an on/off switch (i.e., no electronic speed control), and it was measured without any mechanical loading on the drill shaft.

Full-bandwidth pulse shapes. The random nature of the timing and amplitude of the electrical impulses from the drill made it impossible to use a sampling oscilloscope to measure the emitted impulses. Therefore, no full-bandwidth pulse shape measurements were made, and no FFT spectrum could be derived from the pulse.

Narrowband peak emission spectra. The energy radiated from the electric drill was measured by the spectrum analyzer over the 0.6-5.0 GHz range (Figure 8.82), including a noticeable “bulge” in the 3.1-4.2 GHz range. The highest frequency of measurable signal is not known. The apparent change of amplitudes measured with various bandwidths using the peak detector seems to be about 42 dB for a 2.5-decade change in bandwidth, i.e., a $17 \log_{10} B$ trend line.

Gating, PRR, and modulation. Figure 8.83 shows the gradually building and declining burst of noise that occurs about every 17 ms and is related to the 60 Hz power line frequency.

APDs. Each drill APD in Figure 8.84 appears to be divided into impulsive and noise-like parts, with the noise-like portion determined by measurement system noise and following a $10 \log_{10} B$ rule. The impulsive portion, unlike typical UWB devices, assumes a steep, straight-line slope without any hint of a plateau. The 1-MHz and 3-MHz APDs seem to develop an even steeper slope at the low-probability end, beginning at the 0.1% point. The APDs were only measured to .001% (100 k samples); it is likely that the peak values for the wider bandwidths might have been considerably higher (perhaps 10 dB higher?) had they been extended to the left-hand edge of the graph. The drill APDs are somewhat problematic, since the peak amplitudes of apparently independent pulses do not increase as rapidly as $20 \log_{10} B$. In addition, the very steep slope of the low-probability end makes the measured peak very dependent on the sample size.

Detector summary. The drill detector summary (Figure 8.85) shows that the relative values of the various detectors remain almost the same for all bandwidths; all detectors follow a $10 \log_{10} B$ rule. This behavior fails to match the RF spectrum graphs, which show the peak dB values increasing with a $17 \log_{10} B$ trend line. This discrepancy can be partly explained because the peak measurements for the wider bandwidth spectrum measurements contained a much larger number of independent samples than the narrower bandwidths, which substantially increased the wider bandwidth peak values. It is also likely that the number of “pulses” seen in the drill emission increases proportionately with measurement bandwidth—a much different statistical process than a typical UWB signal (which has a constant number of pulses for wider bandwidths). The Part 15 measurements were too close to system noise to be useful.

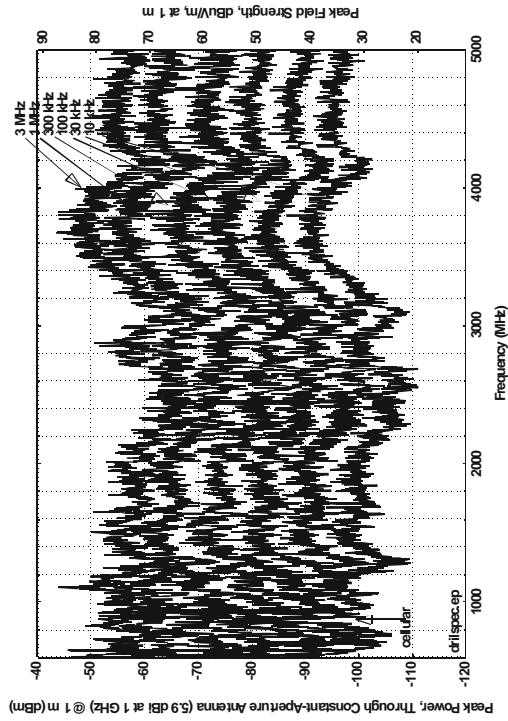


Figure 8.82. Electric drill spectrum as function of measurement bandwidth.

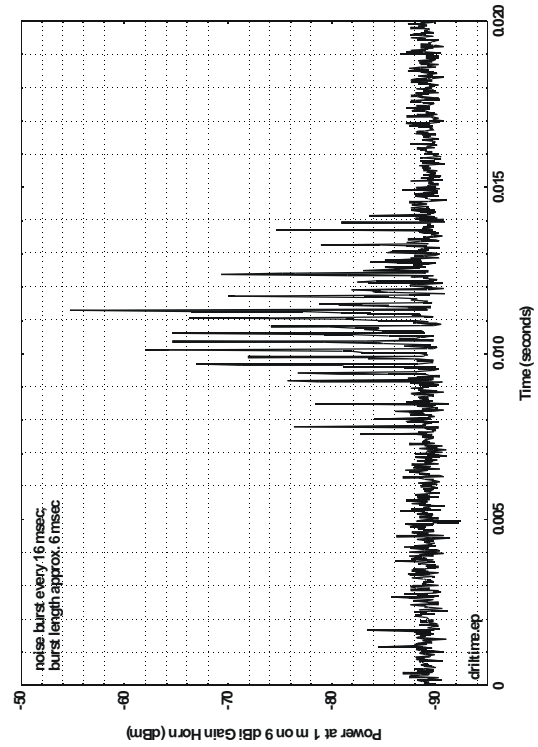


Figure 8.83. Typical electrical drill pulse train.

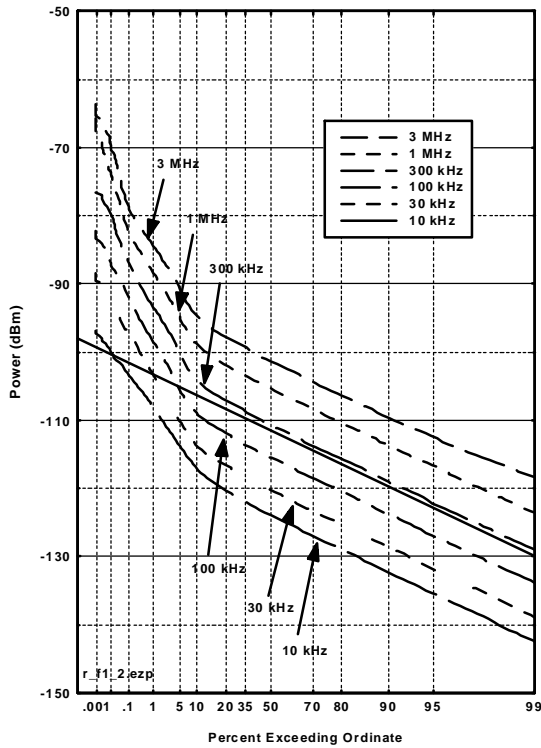


Figure 8.84. Electric drill APDs.

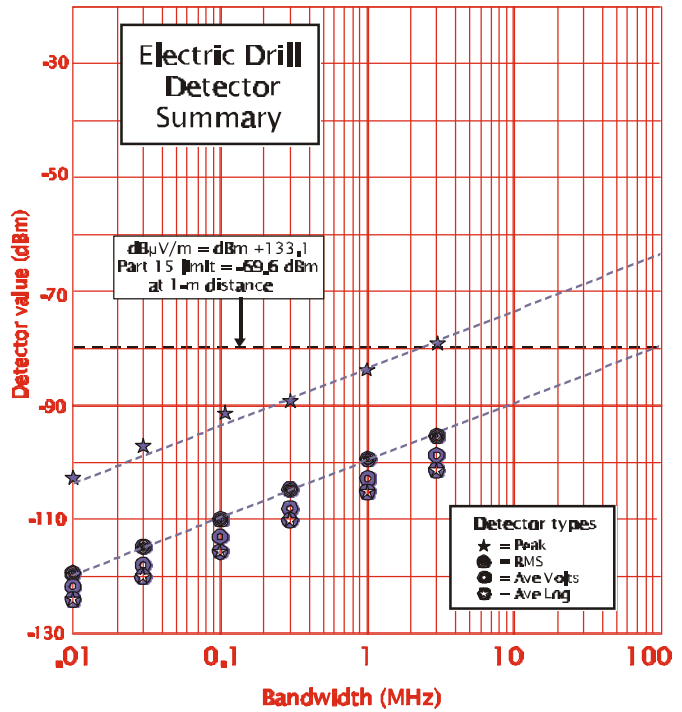


Figure 8.85. Electric drill detector summary.

8.4 Measurement Conclusions

1. The field strength in a bandwidth derived from an FFT of a full bandwidth pulse shape measurement matches the field strength shape measured in a narrower bandwidth by a spectrum analyzer in general shape and absolute amplitude at the peak emission frequency. This confirms that narrowband spectral measurements with a spectrum analyzer or other measurement receiver can be expected to provide accurate information to characterize the overall shape and absolute amplitude of the RF spectrum of UWB signals.
2. Specialized facilities and expertise are needed to obtain accurate measurements of full bandwidth pulse shape. Some of the possible errors associated with this technique are subtle, and many test labs may find that a comparison between FFT-derived spectra and band-limited spectrum analyzer measurements is the only way to verify the accuracy of the full bandwidth pulse shape measurements.
3. There appears to be no simple and accurate technique for relating full bandwidth pulse width data to the 10-dB or 20-dB emission spectra. This is especially true when the UWB pulse is used to excite multiple resonant elements, producing an RF pulse with a multi-lobed ringing response.
4. Amplitude probability distributions (APDs) made with multiple bandwidths provide a useful and theoretically consistent description of UWB signals and how they would affect receivers having various bandwidths. Various detector functions (peak, RMS, average voltage, and average logarithm) can be computed from the APDs or measured directly (if the measurement instrument has the appropriate capabilities).
5. For most UWB devices, the recommended FCC Part 15 non-quasi-peak measurement procedure produces results identical to the average logarithm derived from the 1-MHz bandwidth APD. In situations where the previous statement is not true, the discrepancy is due to insufficient video filtering allowing amplitude variations caused by long-duration duty-cycle events (e.g., gating) to get through to the peak detector.
6. The value measured with an average logarithm detector is substantially affected by measurement system noise for gated or impulsive signals. The average logarithm value is mostly insensitive to energy contained in low-duty-cycle, high-amplitude signals. This results in Part 15 measurement values that can be substantially lower (10-15 dB) than the RMS value (average power) in the UWB signal.
7. The RMS value produces results that are proportional to measurement bandwidth and spectral power density, irrespective of PRR or modulation. Depending on the integration time selected for an RMS measurement, the RMS value can be properly associated with average power when a gated signal is gated on, average power across an entire gating cycle, or average power during other operational periods.

8. Based on measurements of Device C, it seems possible to develop modulation techniques that could cause a UWB signal to look impulsive/gated in a 1-MHz bandwidth and like a CW signal in a 50-MHz bandwidth. Such signals could pass the 1-MHz Part 15 average limit (slipping high-power impulsive signals through the Part 15 average logarithm detector) and the 50-MHz 20-dB peak-to-average limit, while containing average power 15-20 dB above the Part 15 numerical limits. In fact, a signal could probably be designed so that its average power would be within a few dB of the peak level permitted in a 50-MHz bandwidth, while still passing the 1-MHz Part 15 average logarithm limit.

9. A Part 15 average limit based on RMS values would not have the problems described in #6, #7, and #8.

10. Many UWB devices employ dithering, which make their emissions appear more like Gaussian noise (for bandwidths less than the PRR). While this technique is at least partially successful, the specific modulation and dithering techniques may leave a spectrum fine structure that contains many low-level discrete spectral lines and/or other time or frequency distributions that are significantly different from Gaussian behavior. Some of these non-Gaussian characteristics may tend to disappear when actual data are transmitted by UWB devices used for communications, but this effort did not test UWB devices under these conditions.

11. For UWB signals measured with a spectrum analyzer using bandwidths larger than the average PRR, the peak measured values varied according to a $20 \log_{10} B$ rule.

12. Spectrum analyzers having a 50-MHz bandwidth are not yet readily available at test laboratories. A 20-MHz measurement bandwidth was the largest spectrum analyzer bandwidth used in these tests to make peak measurements. Based on #11, a useful alternative to making peak measurements in a 50-MHz bandwidth may be to make measurements in a smaller bandwidth (but large enough that the UWB signal looks impulsive) and to extrapolate to a 50-MHz bandwidth using a $20 \log_{10} B$ rule.

13. We encountered a wide variation of center frequencies (300 MHz to 5 GHz), spectral shapes (very broad to quite narrow), PRR (10 kHz to 10 MHz), modulation techniques (none, absolute dither, relative dither, on-off), gating structures (none, 20%-90%), power levels, and operational functions (short-range to long-range sensing, one-way and two-way communications).

14. Based on measurements of a small sample of existing UWB devices, we are unable to easily or confidently assign UWB devices to a limited number of operational categories having certain distinctive technical characteristics. Therefore, it seems unwise to base any proposed regulations on the assumption that future UWB devices will limit themselves to a few applications and techniques that have been currently developed and demonstrated. Instead, it should be assumed that designers of future UWB devices will creatively explore many additional extensions and combinations of these technologies, and that any UWB device permitted by the regulations will eventually be developed -- possibly in large quantities.

15. Based on measurements of multiple UWB devices, as well as theoretical considerations, the following model (Figure 8.86) describes idealized detector response rules for peak and RMS detectors. This is an idealized treatment, which may or may not apply exactly to specific real systems. One assumption is that the UWB dithering or modulation produces a signal whose narrowband statistics are indistinguishable from Gaussian noise. Actual real-world dithering techniques may or may not approach this ideal, and some UWB devices (e.g., Device C) use dithering techniques whose narrow bandwidth results are quite non-Gaussian. The model assumes that the total number of pulses/s remains equal to the PRR; i.e., that neither gating, on-off keying (OOK), or other dithering/modulation techniques significantly changes the total number of pulses emitted.

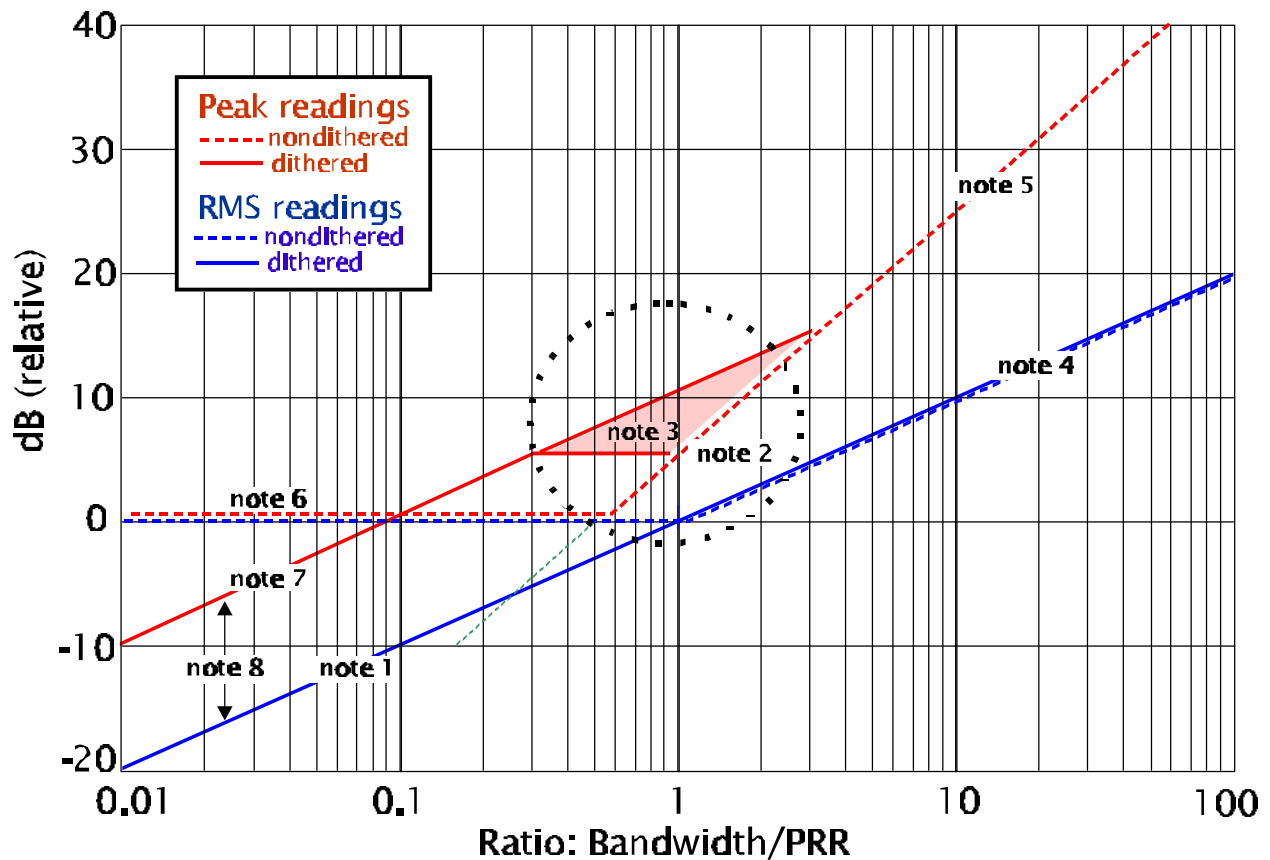


Figure 8.86. Idealized peak and RMS detector values model.

Figure 8.86 describes how a UWB signal measured with peak or RMS detectors in a given a bandwidth can be converted to corresponding readings in another bandwidth. This graph is referenced to the ratio of receiver bandwidth, B , to pulse repetition rate, PRR . This ratio (rather than any particular bandwidth or PRR) is what is critical in determining the rules that govern detector readings. Values of $B/PRR \gg 1$ give non-overlapping impulse responses (the impulsive region). Values of $B/PRR \ll 1$ give overlapping responses that look like Gaussian

noise (dithered case) or discrete CW lines (non-dithered case). Values of $B/PRR = 1$ represent transitional cases, whose behavior varies depending on the details of the modulation on the PRR. The figure shows readings for peak and RMS detectors, for dithered and non-dithered UWB signals. The figure assumes that no gating is present. If gating is present, the figure should be modified by reducing all RMS readings by $10 \log D$, where D is the gating duty cycle, and leaving all peak readings unchanged. The following notes expand on several of the details of the figure.

Note 1. The dithered RMS detector response strictly follows a $10 \log_{10} B$ line, since it is assumed that the total power intercepted by the measurement receiver is strictly proportional to receiver bandwidth. This will be the case for dithered UWB signals for all B/PRR ratios, as well as for B/PRR substantially greater than 1 for the non-dithered case, where the number of discrete CW lines within a bandwidth is proportional to the value of B .

Note 2. The detailed shape of all of these curves near the transition value $B/PRR = 1$ is not well known. It will depend substantially on the details of the UWB device modulation and receiver bandwidth filter response. Filter shapes with sharp suppression of adjacent channel responses will typically have an extended time response and a smaller peak value (i.e., will appear like a smaller bandwidth with respect to the peak value and the duration of the pulse). In general, the slope of the various response curves is trustworthy for bandwidth values far away from the transition point, but neither the exact shape of the transition curves nor the straight-line intercepts between the noise-like and impulse-like regions have been precisely determined for a variety of bandpass characteristics and UWB modulations..

Note 3. The behavior near the transition region where $B/PRR = 1$ for “dithered peak” is particularly obscure. This is partly because there is a transition between a Gaussian probabilistic region and a deterministic impulsive environment. The area in the shaded triangle represents a range of responses that has been observed in this set of measurements, but this region should be examined more carefully. Some measured systems show a very tight grouping of detector readings (4-5 dB difference between average log and peak) when $B/PRR = 1$, while other systems do not.

Note 4. Since impulses have no time overlap in the impulsive region ($B/PRR \gg 1$), there is no difference in responses between dithered and non-dithered pulses. Therefore, the dithered and non-dithered RMS curves will overlay exactly in the $B/PRR \gg 1$ region, and both will follow a $10 \log_{10} B$ slope.

Note 5. For the same reasons described in note 3, the dithered and non-dithered peak curves will overlay exactly in the $B/PRR \gg 1$ region, and both will follow a $20 \log_{10} B$ slope.

Note 6. The response for non-dithered UWB pulses produces evenly-spaced discrete CW lines when $B/PRR \ll 1$. The graph assumes that measurements are made centered on one of the discrete CW lines. Since the envelope response for a single CW line is a constant voltage, the peak and RMS detectors give the same response. Moreover, since the voltage remains constant

for all bandwidths (assuming that the measurement bandpass remains centered on the CW signal), the common response for peak and RMS detectors follows a single horizontal line for $B/PRR \ll 1$.

Note 7. The value of the dithered peak reading will be about 10 dB above the value of the dithered RMS reading. This is based on the assumption that dithering produces statistics identical to Gaussian noise for $B/PRR \ll 1$. Also, see Note 8.

Note 8. It should be noted that the ratio between peak and RMS for detected Gaussian noise is not a constant; instead, it is a statistical quantity that depends on the number of independent observations. For example, there is a 1% chance that the peak will exceed the RMS by about 7 dB, a 0.1% chance of exceeding the RMS by about 8.5 dB, a 0.01% chance of exceeding the RMS by about 10 dB, etc. Therefore, the 10-dB peak-to-RMS ratio is based on collecting the peak reading from 10,000 independent observations. The peak-to-RMS ratio may need to be adjusted to use other probabilities, depending on the exact circumstances of how the model is to be applied.